Article

Serpina3k lactylation protects from cardiac ischemia reperfusion injury

Le Wang[1,2], Dandan Li[1], Fang Yao[1,3], Shanshan Feng[1], Chao Tong[1], Rongjia Rao[1], Meiyan Zhong[3], Xianqiang Wang[4], Wei Feng[4], Zhan Hu[4], Bo Jin[2], Li Wang [1,3], Shengshou Hu[1,3,4] ✉ & Bingying Zhou [1,3] ✉

Lactate produced during ischemia-reperfusion injury is known to promote lactylation of proteins, which play controversial roles. By analyzing the lacty-lomes and proteomes of mouse myocardium during ischemia-reperfusion injury using mass spectrometry, we show that both Serpina3k protein expression and its lactylation at lysine 351 are increased upon reperfusion. Both Serpina3k and its human homolog, SERPINA3, are abundantly expressed in cardiac fibroblasts, but not in cardiomyocytes. Biochemically, lactylation of Serpina3k enhances protein stability. Using Serpina3k knockout mice and mice overexpressing its lactylation-deficient mutant, we find that Serpina3k protects from cardiac injury in a lysine 351 lactylation-dependent manner. Mechanistically, ischemia-reperfusion-stimulated fibroblasts secrete Serpina3k/SERPINA3, and protect cardiomyocytes from reperfusion-induced apoptosis in a paracrine fashion, partially through the activation of cardioprotective reperfusion injury salvage kinase and survivor activating factor enhancement pathways. Our results demonstrate the pivotal role of protein lactylation in cardiac ischemia-reperfusion injury, which may hold therapeutic value.

Myocardial reperfusion therapy is the restoration of myocardial blood flow following an acute myocardial infarction (MI) via thrombolytic or percutaneous coronary intervention, and is established as the standard strategy for reducing infarct size and improving prognosis of MI patients. Paradoxically, however, restoration of blood flow can exacerbate cellular dysfunction and death, and compromise cardiac function and structure in a mechanistically distinct manner, which is termed ischemia-reperfusion (I/R) injury (IRI), a pathophysiological condition that can give rise to various additional heart disorders and even death[1–3]. The pathophysiological mechanisms of myocardial IRI are complex and diverse, including excess production of reactive oxygen species (ROS), apoptosis, autophagy, inflammatory response, mitochondrial dysfunction, and immune response[4]. Various pharmacological and non-pharmacological therapeutic interventions aimed at reducing reperfusion injury, such as cyclosporine A[5,6], N-acetylcysteine (NAC)[7,8], and remote ischemic conditioning[9], have shown limited efficacy in patients, which is possibly the result of incomplete understanding of the global landscape of molecular changes. Therefore, thorough profiling of the molecular mechanisms underlying the pathophysiological changes in I/R may provide unbiased evaluation of the most disease-relevant changes that can be exploited therapeutically.

One of the most prominent consequences of cardiac ischemia is the change in the cardiac metabolic pattern. L-lactate is produced in large quantities in response to MI and I/R, and its roles in these processes are controversial[10–14]. In recent years, lactate is recognized to participate in the posttranslational modification of proteins, by adding

[1]State Key Laboratory of Cardiovascular Disease, Fuwai Hospital, National Center for Cardiovascular Diseases, Chinese Academy of Medical Sciences and Peking Union Medical College, Beijing 100037, China. [2]Department of Clinical Laboratory, Peking University First Hospital, Beijing, China. [3]Shenzhen Key Laboratory of Cardiovascular Disease, Fuwai Hospital Chinese Academy of Medical Sciences, Shenzhen, Shenzhen, China. [4]Department of Cardiac Surgery, Fuwai Hospital, National Center for Cardiovascular Diseases, Chinese Academy of Medical Sciences and Peking Union Medical College, Beijing, China. ✉e-mail: huss@fuwai.pumc.edu.cn; zhouby@fuwai.pumc.edu.cn

a lactyl group to lysine residues[15]. Importantly, lactylation of proteins, including histones and non-histone proteins, are implicated in the epigenetic regulation of gene expression, and are thus involved in a variety of disease conditions[10,12,14,16–19]. Several studies indicated a cardioprotective effect of protein lactylation in cardiac disorders. For example, α-myosin heavy chain (α-MHC) lactylation at K1897 enhanced its interaction with titin, preventing angiotensin infusion-induced heart failure in mice[20]. Following MI, histone H3 lactylation at K18 was reported to trigger a reparative program involving target genes such as *Lrg1*, *Vegf-a*, and *IL-10*[11]. In IRI, histone H3 lactylation at K56 in cardiomyocytes mediated the cardioprotective effects of HSPA12A[21]. Nevertheless, some studies suggest a detrimental role of lactylation in heart disease. Snail family transcriptional repressor 1 (*Snai1*) lactylation mediated lactate-induced endothelial-to-mesenchymal transition to exacerbate cardiac dysfunction in MI, while silencing of *Snail1* or the lactate transporter MCT1 mitigated the harmful effects of lactate[14]. These divergent roles of lactate and protein lactylation in cardiac ischemia prompted us to decipher the lactylome in I/R injury, which may cast light on potential preventative measures in reperfusion therapy.

Therefore, we performed global lactylome and proteome profiling in mice that underwent MI or I/R surgeries. Our data revealed K351-lactylated Serpina3k (SA3K-K351la) as one of the most profoundly altered proteins, specifically in I/R. SA3K-K351la exhibited markedly enhanced protein stability. SA3K was critical to the maintenance of cardiac function during I/R, and K351la was essential for this cardioprotective effect. We determined cardiac fibroblasts (FBs) as the major cellular source of SA3K. Secretion of lactylated SA3K from FBs protected cardiomyocytes (CMs) from I/R-induced apoptosis through inhibiting the WNT pathway, and activating cardioprotective reperfusion injury salvage kinase (RISK) and survivor activating factor enhancement (SAFE) pathways. In summary, our findings identified FB-secreted SA3K as a potent cardioprotectant in IRI, and highlighted the contribution of lactate in this process.

Results

Global lactylome profiling of myocardial ischemia/reperfusion injury

To comprehensively characterize the global protein lysine lactylation (Kla) status in infarcted and reperfused hearts, we performed global lactylome and proteome analyses using a robust, four-dimensional (4D) label-free quantification approach (Fig. 1a). 4D proteomics integrates a fourth dimension, i.e., ion mobility, into the 3 dimensions of classic proteomics, improving peptide and protein identification[22]. Nine-week-old mice were subjected to sham treatment (Sham), myocardial infarction (MI) 30 min or cardiac ischemia/reperfusion (I/R) for 6 h. The selection of the timing was based on previous studies in MI mice[23–25], as well as reports supporting the analysis of protein lactylation within 12 h post stimulation[15]. In lactylome profiling, we identified a total of 1674 Kla sites on 380 proteins, of which 1472 Kla sites from 333 proteins were quantified (Supplementary Table S1; Supplementary Data 1 and 2). Proteomic analysis identified 3279 proteins, 2759 of which were quantified after applying strict filters (Supplementary Table S1; Supplementary Data 3). Normalization of the lactylome data was performed by dividing the relative quantitative value of the modified peptide by that of the corresponding protein from the proteome. In both lactylome and proteome analyses, most peptides consisted of 7-20 amino acids, meeting the quality control requirements (Supplementary Fig. 1a, b). Principal component analysis showed that both the lactylome and proteome of the I/R group diverted from Sham and MI groups, indicating greater alterations occurring at this stage (Supplementary Fig. 1c, d). Pearson correlation analysis revealed that Sham and MI shared greater similarity, while I/R samples exhibited more pronounced deviation from MI and Sham in both the lactylome and proteome (Supplementary Fig. 1e). The relative

standard deviations were higher in the lactylomes compared to the proteomes, but they all remained below the acceptance threshold of 30%[26–28] (Supplementary Fig. 1f, g). To investigate the nature of Kla in the heart, we used the MoMo tool (motif-x algorithm)[29] from the MEME suite to uncover over-represented motifs near identified lactylation sites. Alanine (A) in the -4 position (xxxxxxAxxx_K_xxxxxxxxxx) and lysine (K) in the +7 position (xxxxxxxxxx_K_xxxxxxKxxx) were identified as significantly overrepresented motifs for lactylation (Motif scores 7.77 and 6.87, respectively) (Supplementary Table S2; Supplementary Data 4). The frequencies of individual amino acids occurring near lactylation sites were visualized as a heatmap. Lysine (K) residues were enriched in the −10 and +7 positions, alanine (A) residues in the −6, −4 and +4 positions, and glycine (G) in the −1 position (Supplementary Fig. 1h; Supplementary Data 5). We also used iceLogo to survey amino acids surrounding lactylation sites, and observed similar patterns (Supplementary Fig. 1i; Supplementary Data 6). To determine whether Kla showed any preferences for specific protein structural features, we calculated the probabilities of Kla in alpha-helices, beta strands and coils using NetSurfP, and failed to identify any preference, suggesting that the secondary structures of proteins did not affect lactylation of the target lysine residues (Supplementary Fig. 1j; Supplementary Data 7). Accordingly, the surface accessibilities of all lysine residues and lactylated ones were nearly identical.

We then inspected global Kla distribution changes in MI and I/R, respectively, compared to Sham. In MI, approximately 2.3% proteins exhibited upregulated lactylation, whereas only approximately 0.5% displayed decreased lactylation. Similarly, in I/R, approximately 4.3% of proteins demonstrated upregulated lactylation, whereas only approximately 0.3% displayed reduced lactylation (Fig. 1b; Supplementary Data 8). These results suggest that MI and I/R primarily induced protein lactylation. Proteomic changes resembled changes in the lactylome, with more protein increasing in abundance in MI and I/R, respectively, compared to downregulated proteins (Fig. 1c; Supplementary Data 9). Using more stringent cutoffs (log2 ratio = 1.3), we further quantified the numbers of Kla sites and proteins whose Kla status changed upon MI and I/R. In MI, there were 25 upregulated and 2 downregulated Kla sites, corresponding to 18 and 2 proteins with upregulated and downregulated Kla, respectively. In comparison, there were 71 upregulated and 2 downregulated Kla sites, corresponding to 41 and 2 proteins with upregulated and downregulated Kla, respectively, in I/R, suggesting the continued impact of lactylation after reperfusion (Fig. 1d; Supplementary Data 10). In proteomic analysis, there were 19 and 111 upregulated proteins in MI and I/R groups, respectively (Fig. 1e; Supplementary Data 11). The I/R group had an additional 26 downregulated proteins (Fig. 1e).

Next, we sought to investigate significantly differentially lactylated proteins and differentially expressed proteins during MI and I/R, and performed Gene Ontology analysis to gain insight into their functional relevance. Lactylated proteins were grouped into three distinct clusters based on their lactylation status over time (Fig. 1f; Supplementary Data 12). The first group of proteins (lactylome Cluster 1, C1) was marked by a negligible increase during MI, followed by a surge upon I/R (Supplementary Fig. 2a). Many proteins related to cellular respiration (e.g., Mdh1, Sdha, and Ndufs1), fatty acid oxidation (e.g., Acadm, Hadh, and Echs1), and adult heart development (e.g., Ttn, Myh6, and Myh7) were the founding members of this cluster, suggesting that proteins involved in energy metabolism and contraction were tightly regulated by lactylation during IRI (Fig. 1g and Supplementary Fig. 2a; Supplementary Data 13). Interestingly, C1 also included proteins related to negative regulation of endopeptidase and hydrolase activity, including Serpina3k (SA3K) and Serpina1b (Fig. 1g and Supplementary Fig. 2a; Supplementary Data 13). The second set of proteins (lactylome C2) exhibited increased lactylation during MI, followed by a drop upon reperfusion (Supplementary Fig. 2a), which included proteins involved
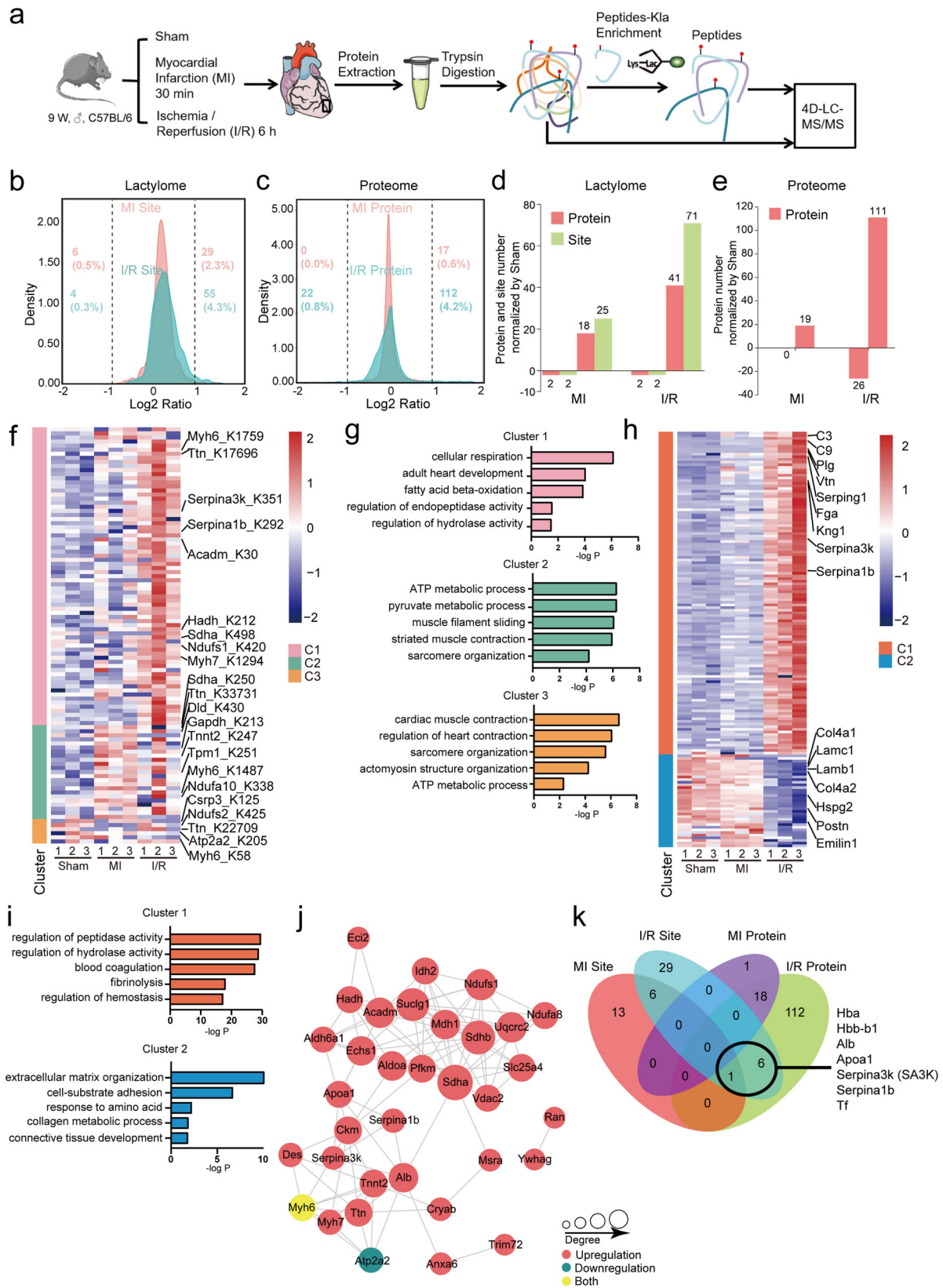
in ATP and pyruvate metabolic processes (e.g., Dld, Gapdh, and Pkfm), as well as ones engaged in muscle filament sliding and sarcomere organization (e.g., Tnnt2, Ttn, and Myh6) (Fig. 1g and Supplementary Fig. 2a; Supplementary Data 13). The third group (lactylome C3) consisted of sarcomeric proteins (Csrp3, Ttn, Atp2a2, and Myh6) and Ndufs2, which displayed the least changes over time (Fig. 1g and Supplementary

Supplementary Fig. 2a; Supplementary Data 13). Notably, all three clusters shared Ttn and Myh6, due to their lactylation at multiple sites. The vast overrepresentation of respiratory and contractile components in the lactylome suggested that they were the major substrates of endogenous lactylation during I/R stress. Differentially expressed proteins were clustered into two opposing trends (Fig. 1h; Supplementary

Fig. 1 | Global lactylome profiling of myocardial ischemia/reperfusion injury.
a Experimental design. Adult C57BL/6 mice were subjected to sham, myocardial infarction (MI) or ischemia/reperfusion injury (I/R) surgeries, respectively. Protein extracted from the infarct area was used for global proteome and lactylome profiling by 4D-LC-MS/MS. $n = 3$ biological replicates, each biological replicate was a pooled myocardial sample from 3 mice. **b, c** Density gradient diagram of the Log_2 ratios of Kla sites and proteins in MI and I/R groups of the lactylomes (**b**) and proteomes (**c**), respectively. Red and green represent MI and I/R groups, respectively. Red and green numbers (percentages) represent the numbers and percentages of up- or down-regulated Kla sites or proteins, respectively (cutoff $|Log_2FC| > 1$). **d** Numbers of Kla sites and Kla proteins exhibiting significant Kla-level changes after MI and I/R (cutoff of $|Log_2FC| > 1.3$). **e** Numbers of proteins or sites exhibiting significant expression changes after MI and I/R (cutoff of $|Log_2FC| > 1.3$). **f** Heat map showing hierarchical

clustering of differentially lactylated sites in Sham, MI and I/R mouse hearts. Three biological replicates are shown separately. **g** Gene ontology (GO) analyses of enriched biological processes in (**f**). Selected top categories are shown. Statistical significance was performed using the two-sided hypergeometric distribution test. **h** Heat map showing hierarchical clustering of differentially expressed proteins in Sham, MI and I/R mouse hearts. Three biological replicates are shown separately. **i** Gene ontology (GO) analyses of enriched biological processes in (**h**). Selected top categories are shown. Statistical significance was performed using the two-sided hypergeometric distribution test. **j** Protein-protein interaction network of lactylated proteins in I/R based on the STRING database. The size of the circles represents the number of interacting proteins. Red represents upregulation, green represents downregulation, and yellow represents both. **k** Venn diagram of differentially expressed or lactylated proteins in MI or I/R compared to Sham control.

Data 14). Proteome cluster 1 (C1) showed a pattern highly similar to lactylome C1, while proteome C2 first mildly decreased during MI and then quickly dropped in I/R (Supplementary Fig. 2b). Interestingly, negative regulators of peptidase and hydrolase activities, including SA3K, Serpina1b and Serping1, were among the most strongly upregulated proteins (Fig. 1i; Supplementary Data 15). These proteins are known to function as serine protease inhibitors that assist in blocking the activity of certain digestive enzymes, and are associated with cardiovascular diseases due to their regulatory roles in blood clotting, inflammation, and oxidative stress[30,31]. The observation that I/R-specific differentially lactylated and expressed proteins both exhibited enrichment in serine-type endopeptidase inhibitor activity indicated that serpin family proteins may play an important role in I/R (Supplementary Fig. 2c, Supplementary Data 16). On the contrary, downregulated proteins were almost exclusively extracellular matrix (ECM) proteins, suggesting tremendous breakdown and remodeling of the ECM, a known consequence of I/R damage[32] (Fig. 1i; Supplementary Data 15).

To further understand the relationship among differentially lactylated proteins in I/R compared to Sham, we used STRING to delineate their functional or physical interactions. As anticipated, there were two major sets of proteins: a set associated with sarcomeric structures (e.g., Tnnt2, Ttn, Myh7, Myh6, and Desmin), and another large group related to metabolism (e.g., Ckm, Pfkm, Mdh1, Sdha, Sdhb, Ndufs1, Ndufa8, and Slc25a4) (Fig. 1j; Supplementary Data 17). The two members of the serpin family, SA3K and Serpina1b, were associated with proteins in the blood, including Apoa1 and Alb. Serpina3k was additionally functionally associated with Myh6 (cardiac α-myosin heavy chain) and Ckm (creatine kinase, M-type), suggesting a potential role of SA3K in the myocardium.

Next, we overlapped significantly changed proteins in MI and I/R in both the lactylome and proteome. Strikingly, there was almost no overlap among the four sets of proteins except for the 7 shared ones between proteins with significantly altered lactylation status and proteins significantly changed in their expression during I/R, including hemoglobin alpha chain complex (Hba), hemoglobin beta adult major chain (Hbb-b1), albumin (Alb), apolipoprotein A1 (Apoa1), SA3K, Serpina1b, and transferrin (Tf) (Fig. 1k; Supplementary Data 18). Among them, Hba, Hbb-b1, Alb, Apoa1, and Tf are proteins highly abundant in the blood. Strikingly, the remaining two proteins were SA3K and Serpina1b, suggesting their prominent and specific roles in I/R. The only human homolog of the family of closely related murine Serpina3 proteins (one of them being SA3K)[33], SERPINA3 (SA3), demonstrated efficiency as a predictor of adverse cardiac events in myocardial infarction and heart failure[34,35]. Therefore, we set out to define the pathophysiological function and consequences of SA3K lactylation in I/R.

SA3K and SA3K-Kla is increased upon I/R in vivo and upon normoxia-hypoxia in vitro

To validate the alterations of SA3K protein expression during MI and I/R, we performed western blotting on myocardial specimens from MI

and I/R mouse hearts. SA3K protein exhibited a 4.8-fold increase compared to both Sham and MI, indicating that increased SA3K was an IRI-specific response (Fig. 2a). Consistently, the immunofluorescence signal intensity of SA3K in cardiac sections were significantly higher than those in Sham or MI (Fig. 2b). Further, we validated SA3K lysine lactylation (SA3K-Kla) by immunoprecipitation. SA3K-Kla was significantly and specifically increased in I/R (Fig. 2c, d). Our MS/MS data showed that lactylation of SA3K occurred on residue K351 (Supplementary Fig. 3). To this end, we generated polyclonal antibodies specifically recognizing SA3K-K351la. The specificity and potential cross-reactivity with succinylation of the antibodies were verified by dot blot assays (Supplementary Fig. 4a). In line with above observations, western blotting using the SA3K-K351la-specific antibody confirmed the significant increase in SA3K-K351la level in I/R (Fig. 2e). To examine the time course for SA3K elevation, we harvested cardiac tissue every hour from I/R 0 h through I/R 6 h (Supplementary Fig. 4b). Western blotting of both SA3K-K351la and total SA3K revealed that lactylation levels of K351 rose significantly at I/R 1 h compared to MI, while protein levels started to increase substantially at I/R 2 h, and remained steady until I/R 6 h (Supplementary Fig. 4c–e). Together, these data support a significant and rapid elevation of SA3K lactylation at K351 in the heart after I/R.

The observation that SA3K barely co-localized with cardiomyocyte (CM) marker ACTN2 (Fig. 2b) prompted us to investigate the cellular basis for increased SA3K expression. Immunofluorescence revealed strong co-localization of FB marker vimentin (VIM) with SA3K in I/R (Fig. 2f). We isolated primary neonatal mouse CMs and cardiac FBs, and examined base level SA3K mRNA expression. SA3K was expressed at a significantly higher level in FBs than in CMs (Fig. 2g). Next, we simulated I/R in vitro by culturing FBs and CMs separately under either normoxia (N), hypoxia (H, 1% O_2 for 24 h), or hypoxia-normoxia (H-N, 1% O_2 for 24 h, then normoxia for 12 h). In FBs, both SA3K-K351la and protein levels were specifically and significantly upregulated in H-N (Fig. 2h). By contrast, such increase was absent in CMs (Fig. 2i). To determine the conservation of this phenomenon, we isolated adult human primary CMs and cardiac FBs. In accordance with neonatal mouse cardiac cells, SA3, the human homologue of mouse SA3K[36], was also specifically expressed in FBs (Fig. 2j). Its expression was also specifically upregulated in FBs under H-N (Fig. 2k). Given that SA3 is a secreted protein, we further quantified SA3 in the medium of cultured human FBs by enzyme-linked immunosorbent assay (ELISA), and consistently observed substantial increase in secreted levels of SA3 upon H-N stimulation (Fig. 2l). To further explore whether H-N caused changes in SA3-Kla in human CMs and FBs, we examined SA3-Kla levels by immunoprecipitation. SA3-Kla was markedly elevated in H-N in human FBs, but not under hypoxia or in CMs (Fig. 2m, n). Collectively, these findings indicated that SA3K and its human homologue, SA3, increased at both protein expression and lactylation levels in cardiac FBs upon I/R or H-N injury specifically.
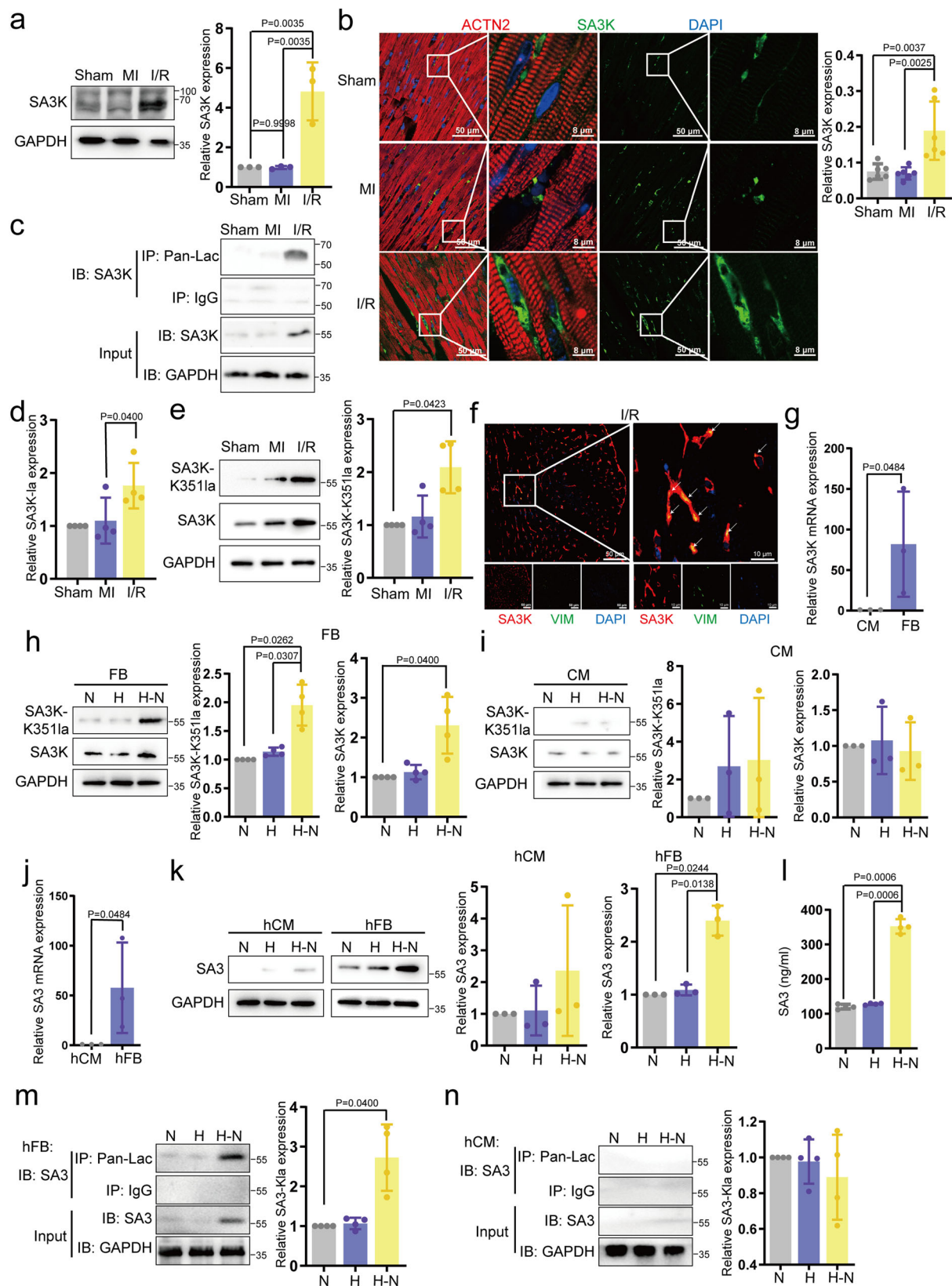
L-lactate upregulates SA3K level by enhancing lactylation-dependent protein stability

To this end, we sought to investigate the molecular basis for the increase in both SA3K protein and lactylation level. We observed that SA3K mRNA was not increased in the infarct zone in mouse hearts upon I/R (Supplementary Fig. 5a). In the same vein, H-N treatment of cultured CMs or FBs also failed to enhance SA3K mRNA level in mice (Supplementary Fig. 5b) or SA3 mRNA level human cells (Supplementary Fig. 5c). These results indicated that elevated SA3K protein was unlikely the result of increased transcription, and led us to speculate that its regulation occurred at the protein level.

Fig. 2 | SA3K and SA3K-Kla is increased upon I/R in vivo and upon normoxia-hypoxia in vitro. a Western blotting and quantification of SA3K protein in mouse heart tissue. $n = 3$ mice per group. **b** Immunostaining and quantification of SA3K expression in mouse heart sections. Scale bar: 50 μm and 8 μm. $n = 6$ mice per group. **c, d** Immunoprecipitation and western blotting (**c**) and quantification (**d**) of the lactylation level of SA3K in mouse heart tissue. $n = 4$ mice per group. **e** Western blotting of SA3K using an SA3K-K351la-specific antibody in mouse heart tissues. Quantification is shown on the right. $n = 4$ mice per group. **f** Immunostaining of SA3K and vimentin (VIM) in mouse I/R heart sections. Arrows indicate co-localization. Scale bar: 50 μm (left) and 8 μm (right). **g** qRT-PCR of SA3K mRNA in neonatal mouse CMs and FBs. $n = 3$ independent experiments. **h, i** Western blotting of SA3K-K351la and SA3K in neonatal mouse FBs (**h**) and CMs (**i**) cultured under normoxia (N), hypoxia (H), or normoxia-hypoxia (H-N) conditions, $n = 4$ (FB) and

$n = 3$ (CM) independent experiments. **j** qRT-PCR of SA3 mRNA in adult human primary CMs and cardiac FBs. $n = 3$ independent experiments. **k** Western blotting and quantification of SA3 expression in adult human primary FBs and CMs cultured under normoxia (N), hypoxia (H), or normoxia-hypoxia (H-N) conditions, $n = 3$ independent experiments. **l** ELISA of SA3 secreted from human primary FBs, $n = 4$ independent experiments. **m, n** Immunoprecipitation and western blotting of the lactylation level of SA3 in adult human primary cardiac FBs (**m**) and CMs (**n**) cultured under different conditions. Quantifications are shown on the right. $n = 4$ independent experiments. Significance was calculated using one-way ANOVA followed by Tukey's multiple comparisons test (**a, c, e, h, k, l**), unpaired, one-tailed t-test (**g, j**), or the Friedman test followed by Dunn's multiple comparisons test (**d, m**). For (**a, c, m, n**), GAPDH loading control was run on a separate gel. All data are means ± SD. Source data are provided as a Source Data file.

We additionally noted that whole tissue L-lactate was significantly upregulated in the infarct areas of the mouse heart upon MI and I/R (Supplementary Fig. 5d). Likewise, intracellular L-lactate was also strongly upregulated by H and H-N in in vitro cultured neonatal mouse CMs and FBs (Supplementary Fig. 3e). These changes in L-lactate production were paralleled with marked increases in lactylated proteins and protein Kla sites (Fig. 1f). Given that previous studies reported protein Kla levels to be affected by lactate[15], and because protein modifications are extensively involved in post-translational regulation of proteins, we hypothesized that L-lactate produced during I/R regulated the stability of SA3K protein through K351 lactylation.

To this end, we first exposed FBs to increasing levels of L-lactate, and observed steady, dose-dependent increases in both SA3K and SA3K-K351la (Fig. 3a), indicating that L-lactate induced the increase in SA3K lactylation and protein expression. As intracellular L-lactate production is contingent on the balance between glycolysis and mitochondrial metabolism, we tested whether the activity of enzymes in these two pathways can modulate L-lactate level and consequent SA3K-K351la (Fig. 3b). As expected, rotenone, an inhibitor of mitochondrial respiratory chain complex I, strongly induced L-lactate production (Fig. 3c), while oxamate, an inhibitor of lactate dehydrogenase (LDH), significantly suppressed L-lactate level (Fig. 3c). Accordingly, oxamate and rotenone dose-dependently decreased and increased SA3K-K351la and SA3K levels, respectively (Fig. 3d, e), further implying that lactate directly regulated SA3K-K351la and SA3K. Together, these findings demonstrated that both exogenous and endogenous lactate regulated SA3K-K351la and SA3K concurrently. The positive correlation between SA3K-K351la and SA3K indicated that SA3K-K351la promoted SA3K protein stability.

To test this idea, we treated cells with cycloheximide (CHX) to inhibit protein synthesis, and quantified protein expression over time, with or without the addition of L-lactate or oxamate. The calculated half-life of SA3K increased from 2.98 h to 6.74 upon L-lactate treatment, and declined to 1.92 h following inhibition of lactate by oxamate (Fig. 3f). In the presence of proteasome inhibitor MG132 and CHX, protein levels remained steady (Fig. 3f), suggesting that lactate played a role in maintaining SA3K protein stability. Similar observations were made in adult human primary FBs, where L-lactate treatment increased SA3 half-life from 4.12 h to 6.36 h, while oxamate treatment reduced SA3 half-life to 2.16 h (Supplementary Fig. 5f). To further assess whether this regulatory effect was mediated by SA3K-K351la, we constructed a mutant, FLAG-tagged form of SA3K (K351R), and compared its expression with the wild-type (WT) recombinant protein. The calculated half-life of exogenous WT-SA3K increased from 4.66 h to 6.71 h upon L-lactate treatment, while the half-life of the SA3K-K351R was almost identical to the WT protein (4.84 h) (Fig. 3g), suggesting that K351la was required for the stabilization of SA3K by lactate.

Acetylation is a common form of post-translational modification that shares biochemical characteristics with lactylation[37]. To rule out the possibility of acetylation (SA3K-Kac) regulating SA3K protein stability, we first examined SA3K-Kac levels in response to increasing or decreasing L-lactate concentrations. Immunoprecipitation showed that changes in neither extracellular L-lactate (L-lactate treatment) nor intracellular lactate (oxamate or rotenone treatment) had an effect on SA3K-Kac (Supplementary Fig. 6a). The addition of 100 μM acetyl CoA into the culture medium slightly enhanced the half-life of endogenous SA3K (3.77 h), but failed to exert any effect on the half-life of exogenous SA3K-WT (4.60 h) (Supplementary Fig. 6b). Taken together, these data indicated that L-lactate inhibited SA3K degradation through SA3K-K351la.

SA3K is an important driver of cardiac protection in reperfusion injury

To directly evaluate the role of SA3K in IRI, we generated SA3K knockout (SA3K-KO) mice (Fig. 4a and Supplementary Fig. 7a). One group of wild-type (WT) mice and 2 groups of SA3K-KO mice were respectively ligated for 30 min, and then reperfused for 6 h to model I/R. In the second group of SA3K-KO mice, recombinant, purified His-tagged SA3K (0.5 mg/kg) was injected at the time of reperfusion (Fig. 4a). 2,3,5-triphenyl tetrazolium chloride (TTC) and Evans blue staining at 1 D post I/R showed that the areas at risk (AAR) were comparable among groups (Fig. 4b, c). However, the AAR-normalized infarct size was significantly increased upon SA3K-KO, which was rescued by injection of recombinant SA3K (Fig. 4d). To assess cardiac injury, we measured serum levels of cardiac troponin T (cTnT), cardiac troponin I (cTnI), and creatine kinase MB (CK-MB). These markers were significantly increased in SA3K-KO mice compared to WT control, and were partially attenuated by the injection of exogenous SA3K (Fig. 4e–g). The fraction of apoptotic cells, assessed by terminal deoxynucleotidyl transferase dUTP nick end labeling (TUNEL) staining, markedly increased in SA3K-deficient mice at 1 D (Fig. 4h), while the injection of SA3K significantly reversed the increase in apoptosis (Fig. 4h). Echocardiographic analysis was performed at multiple time points (baseline, 7 D, 14 D, and 28 D) to evaluate changes in heart function. Baseline heart function of SA3K-KO mice was indistinguishable from that of WT control mice (Supplementary Fig. 7c–h). At 7 D, 14 D and 28 D, the ejection fraction (EF) was severely impaired in SA3K-deficient mice compared to WT control, while His-SA3K injection offered a modest protective effect (Fig. 4i, j, Supplementary Fig. 7b, c). Similar trends were observed with fractional shortening (FS) (Fig. 4j, Supplementary Fig. 7d). Left ventricular end-diastolic volume (LVEDV), left ventricular end-systolic volume (LVESV), left ventricular internal diameter at end diastole (LVIDd) or systole (LVIDs) exhibited pronounced increases at D28 in SA3K-KO mice, indicating ventricular dilatation following I/R, which were partially rescued by supplementation of exogenous His-SA3K (Fig. 4j). Some of these latter parameters exhibited significant changes as early as D7
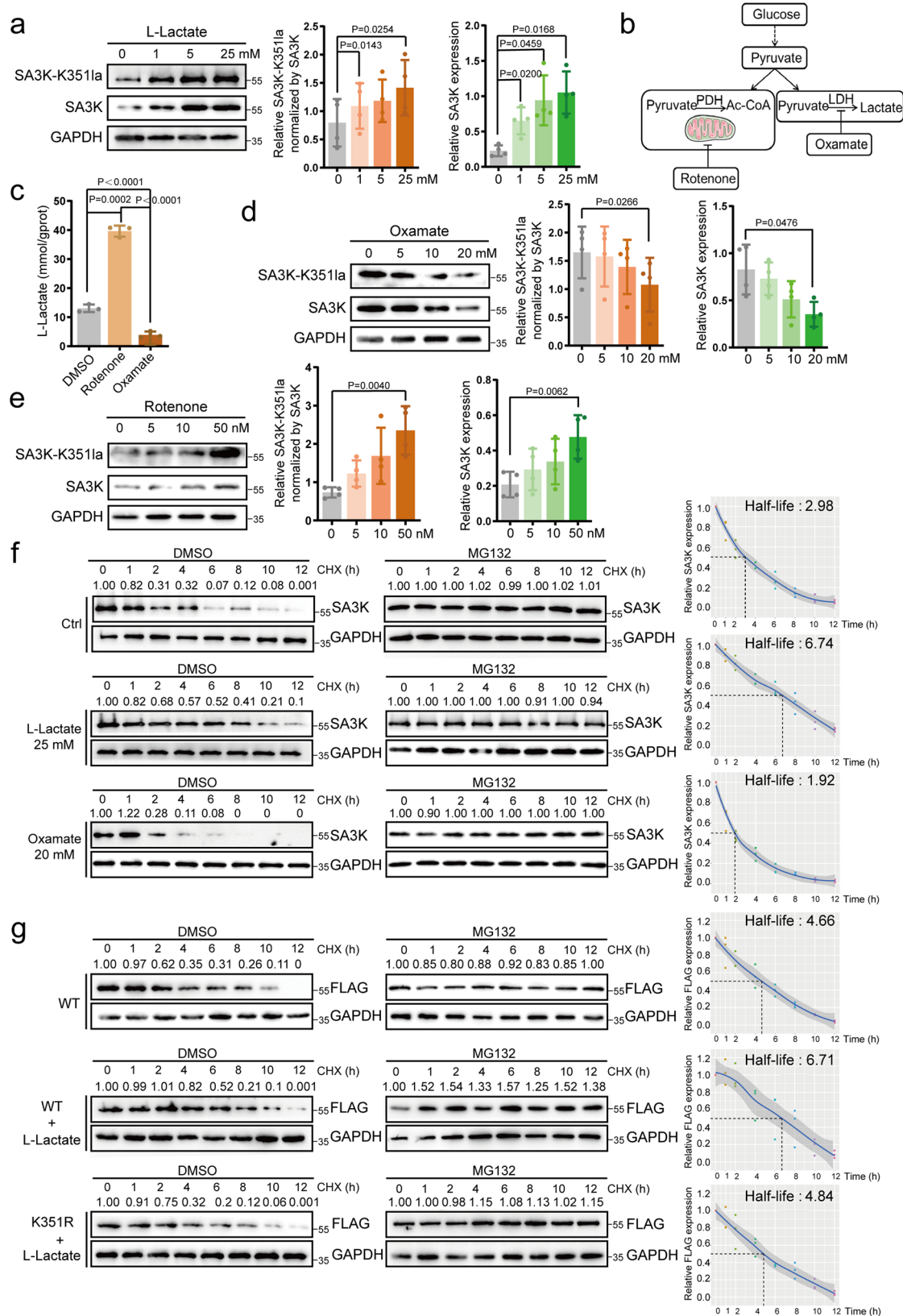
(Supplementary Fig. 7e–h). At 28 D post I/R, we analyzed cardiac fibrosis by Masson's trichrome staining. SA3K-KO hearts exhibited a significant increase in collagen deposition compared to WT hearts, while SA3K injection significantly alleviated fibrosis (Fig. 4k and Supplementary Fig. 7f). Collectively, the above findings indicated that SA3K conferred cardiac protection against IRI.

SA3K lactylation at K351 is required for cardiac protection

To gain insight into the role of SA3K-K351la in cardiac protection, we generated adeno-associated virus serotype 9 (AAV9) expressing either WT (SA3K-WT) or mutant SA3K (SA3K-K351R) under the fibroblast-specific promoter FSP1 (Fig. 5a and Supplementary Fig. 8a). Mice were injected with empty vector (EV), SA3K-WT- or SA3K-K351R-expressing

Fig. 3 | L-lactate upregulates SA3K level by enhancing lactylation-dependent protein stability. a Western blotting of SA3K protein and SA3K-K351la levels in neonatal mouse FBs cultured in increasing concentrations of L-lactate for 24 h. Quantification of relative SA3K and SA3K-K351la expression level is shown on the right. $n = 4$ independent experiments. **b** Schematic of regulatory factors in glucose metabolism. Rotenone inhibits oxidative phosphorylation, while oxamate inhibits lactate production. **c** Intracellular L-lactate levels were measured in mouse neonatal FBs treated with rotenone or oxamate for 24 h. $n = 3$ independent experiments. **d**, **e** Western blotting of SA3K protein and SA3K-K351la levels in mouse neonatal FBs cultured in increasing concentrations of oxamate (**d**) or L-lactate (**e**) for 24 h. GAPDH loading control was run on a separate gel in (**e**). Quantifications of relative SA3K and SA3K-K351la expression level are shown on the right, respectively. $n = 4$ independent experiments. **f** Measurement of endogenous SA3K protein half-life. Neonatal FBs were cultured in control medium, 25 mM L-lactate, or 20 mM oxamate for 24 h, and then treated with 50 μg/ml cycloheximide (CHX) for the indicated times in the presence or absence of MG132 before cellular proteins were extracted for western blotting. Quantitation was done by densitometry and expressed as the signal ratio of SA3K/GAPDH. $n = 3$ independent experiments. **g** Measurement of exogenous SA3K protein half-life. Neonatal FBs were transduced with SA3K-WT- or SA3K-K351R-expressing lentivirus. Cells overexpressing SA3K-WT or SA3K-K351R were treated with 25 mM L-lactate for 24 h, and then treated with 50 μg/ml CHX for the indicated times in the presence or absence of MG132 before cellular proteins were extracted for western blotting. Quantitation was done by densitometry and expressed as the signal ratio of SA3K/GAPDH. $n = 3$ independent experiments. Half-life calculation and visualization were performed by R (4.0.3) and ggplot2 (3.3.2) package in (**f**, **g**). Significance was calculated using one-way ANOVA followed by Tukey's multiple comparisons test (**a**, **c**, **d**, **e**). All data are means ± SD. Source data are provided as a Source Data file.

virus, and IRI was induced using the same method as above (Fig. 5a). At 1 D post I/R, myocardial infarct size was significantly reduced in WT-SA3K mice, compared to EV control, whereas those in SA3K-K351R mice were not significantly different from EV control, suggesting that K351 was indispensable for the protective effect of SA3K (Fig. 5b–d). Serum levels of cTnT, cTnI, and CK-MB were significantly suppressed in SA3K-WT mice, but not in SA3K-K351R mice (Fig. 5e–g). Exogenous expression of SA3K-WT significantly attenuated I/R-induced apoptosis, while SA3K-K351R failed to show any protective effect compared to EV control (Fig. 5h). Echocardiographic analysis showed that virus injection did not perturb baseline cardiac function (Supplementary Fig. 8c–h). SA3K-WT significantly improved cardiac function by 7 D, an effect that lasted through 28 D, whereas SA3K-K351R failed to show any improvement (Fig. 5i, j, Supplementary Fig. 8b–h). Finally, assessment of fibrosis on 28 D showed significant attenuation of fibrosis by SA3K-WT, but not SA3K-K351R (Fig. 5g and Supplementary Fig. 8e). In summary, these data demonstrated that lactylation of SA3K at K351 was essential to the cardioprotective effect of SA3K, suggesting that protein half-life, rather than protein amount, determines IRI protection efficiency.

SA3K secreted by FBs protect CMs from IRI-induced apoptosis through paracrine signaling

Re-analysis of TUNEL staining specifically in CMs (TUNEL$^+$ACTN2$^+$) (Figs. 4h and 5h) revealed that SA3K most pronouncedly altered the apoptosis of CMs (Supplementary Fig. 9a, b). Given that CMs themselves hardly express SA3K (Fig. 2), and because of the minimal response of CM-specific SA3K to H-N (Fig. 2), we hypothesized that FBs protected CMs from IRI via paracrine interaction mediated by SA3K.

To test this hypothesis, we first isolated FBs and CMs from neonatal mice or adult human cardiac tissue, and cultured them separately (Fig. 6a). Conditioned medium from FBs in normoxic or H-N culture were respectively used for CM culture, the latter of which was then challenged by H-N. In a group of CMs receiving H-N conditioned medium, we used a SA3K or SA3 neutralizing antibody (Nab) to determine the role of SA3K/SA3 in the paracrine effect (Fig. 6a). H-N conditioned medium significantly suppressed mouse CM apoptosis, an effect that was abrogated by Nab (Fig. 6b, c). Accordingly, cleaved caspase 3 and Bax levels in mouse CMs were also suppressed by H-N conditioned medium, while medium treated with Nab conferred little protection against CM apoptosis (Fig. 6d, e). Similar observations were also made using adult human primary FBs and CMs (Fig. 6d, e). Further, in both neonatal mouse and adult human cells, H-N conditioned medium significantly suppressed lactate dehydrogenase (LDH) release and enhanced ATP levels, indicating better survival of CMs, which were also abrogated by Nab (Fig. 6f–h). However, cellular reactive oxygen species (ROS) and respiration were minimally affected (Supplementary Fig. 9c, Supplementary Fig. 10). These results suggested that, in

response to IRI, FBs produced a secretome that protected CMs from IRI, an effect that was primarily mediated by SA3K.

To further investigate the protective role of SA3K in IRI, we depleted SA3K in FBs via lentiviral knockdown, and transferred conditioned medium to CM cultures prior to H-N treatment in the latter (Fig. 6i and Supplementary Fig. 9d, e). Compared non-targeting (NT) control, shSA3K#1 significantly increased the fraction of apoptotic cells within the population, while shSA3K#2 also displayed an increasing trend (Fig. 6j, k). Likewise, SA3K depletion also enhanced cleaved caspase 3 and Bax expression, as well as LDH release (Fig. 6l, m Supplementary Fig. 9f). However, ATP levels, ROS and mitochondrial function were not affected (Supplementary Fig. 9g, h, Supplementary Fig. 10). Depletion of SA3 in adult human cardiac FBs also produced similar findings in adult human primary CMs (Fig. 6l, n, Supplementary Fig. 9d–h). Therefore, these findings suggested that SA3K/SA3 secreted by FBs was capable of protecting CMs from IRI-induced apoptosis.

Furthermore, we increased SA3K expression directly in CMs through lentivirus-mediated expression or recombinant His-SA3K supplementation into CM medium (Supplementary Fig. 11a). Significant protection of CMs, marked by downregulated apoptotic markers, was observed following H-N stimulation (Supplementary Fig. 11b, c). This finding showed that SA3K protected CM against apoptosis in response to H-N.

To understand whether this protection depends on K351 lactylation, we ectopically expressed SA3K-WT and SA3K-K351R in FBs, and assessed their protection efficiency (Fig. 6o, Supplementary Fig. 9i, j). Similar to the in vivo data, SA3K-WT significantly suppressed CM apoptosis, while SA3K-K351R failed to show any effect (Fig. 6p, q). SA3K-K351R also failed to suppress cleaved caspase 3 and Bax expression, or LDH release, as the WT form did (Fig. 6r, Supplementary Fig. 9k). Again, ATP levels, ROS and mitochondrial respiration were not affected (Supplementary Fig. 9l, m), suggesting that the regulation of cell death by SA3K was not mediated by mitochondrial impairment. Together, these results underscore the requirement for Kla in CM protection.

In summary, SA3K secreted from FBs during IRI protected CMs from IRI-induced apoptosis through paracrine signaling, which was dependent on lactylation-regulated SA3K protein stability, and not abundance.

SA3K protects CMs by inhibiting the WNT, and activating RISK and SAFE pathways

To explore the molecular mechanism underlying the protective effect of SA3K, we leveraged the experimental design described Fig. 6i, o, and analyzed altered signaling pathways in CMs. We first analyzed the AMPK signaling pathway[38], a classical myocardial protection pathway. However, SA3K/SA3 levels failed to modulate the activity of the AMPK signaling pathway in CMs in mouse or human
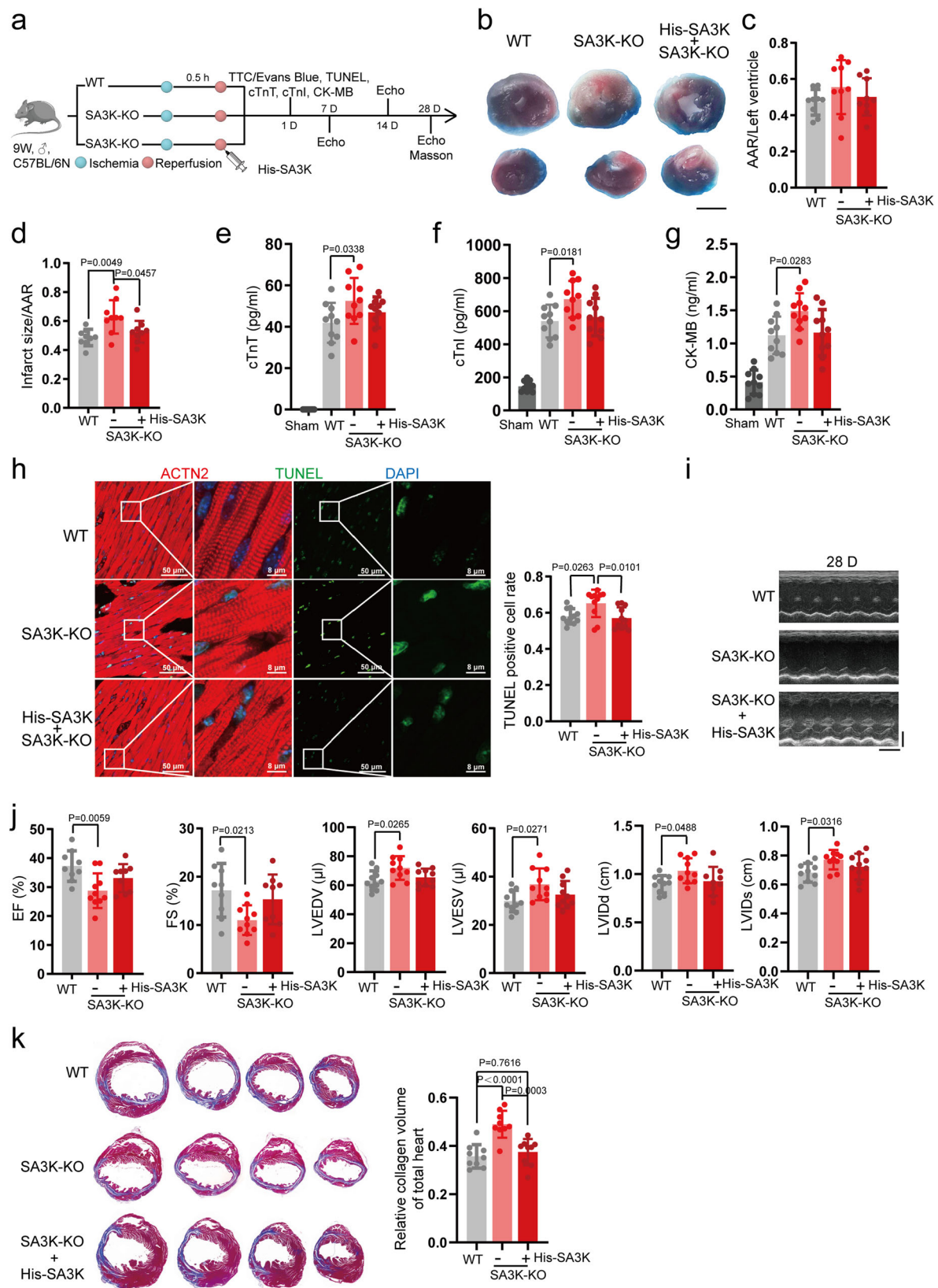
(Supplementary Fig. 12a–f). Further, given that SA3K has been reported to inhibit WNT signaling in angiogenesis[39], we sought to determine whether WNT pathway was altered following changes in SA3K levels. Both phosphorylated LDL receptor-related protein (p-LRP) and β-catenin levels were significantly suppressed upon SA3K overexpression (Supplementary Fig. 12g–i). When treated with conditioned medium from FBs with SA3K depletion, p-LRP increased significantly, while β-catenin also displayed an increasing trend (Supplementary Fig. 12g–i). Conditioned medium from adult human primary FBs with SA3 overexpression or knockdown showed similar, but milder, effects on adult human primary CMs (Supplementary Fig. 12j–l).

Fig. 4 | SA3K is an important driver of cardiac protection in reperfusion injury. a Diagram outlining the experimental design for evaluating SA3K function in I/R. Wild-type (WT) or SA3K knockout (SA3K-KO) mice were subjected to I/R surgery. His-tagged SA3K (His-SA3K) was injected into a group of SA3K-KO at reperfusion. Analyses of myocardial ischemia, apoptosis, cardiac function, and fibrosis were performed at indicated time points. **b** Representative photographs showing TTC-stained transverse sections of Evans blue-perfused hearts. **c, d** Area at risk (AAR) (**c**) and infarct size (**d**) were quantified 1 day after IRI, *n* = 9 mice in each group. **e**–**g** Serum levels of cardiac troponin T (cTnT) (**e**), cardiac troponin I (cTnI) (**f**), and creatine kinase MB (CK-MB) (**g**) were measured 1 day after IRI, *n* = 10 mice in each group. **h** Representative terminal deoxynucleotidyl transferase dUTP nick end labeling (TUNEL) staining images showing apoptotic cell death in heart sections 1 day after IRI. An ACTN2 antibody was used to label cardiomyocytes. Scale bar,

50 μm and 8 μm. Quantification of TUNEL-positive cell rates is shown on the right. *n* = 11 mice in each group, 6 sections per animal. **i** Representative echocardiograms at D28. **j** Quantification of left ventricular ejection fraction (EF), left ventricular fractional shortening (FS), left ventricular end-diastolic volume (LVEDV), left ventricular end-systolic volume (LVESV), left ventricular internal diameter at end diastole (LVIDd), and left ventricular internal diameter at end systole (LVIDs) at D28 based on echocardiography. *n* = 10 mice in each group. **k** Masson's trichrome staining of heart sections 28 days after reperfusion. Scale bar: 2 mm. Quantification of fibrosis is shown on the right. *n* = 9 mice in each group, 4 sections per animal. Significance was calculated using one-way ANOVA followed by Tukey's multiple comparisons test (**d**–**h**, **j**, **k**). All data are means ± SD. Source data are provided as a Source Data file.

Given the pro-survival effect of SA3K, we further tested whether it promoted classical cardioprotective pathways, including reperfusion injury salvage kinase (RISK)[40] and survivor activating factor enhancement (SAFE) pathways[41]. The RISK pathway is a collection of pro-survival kinase pathways, including AKT and ERK1/2, which confers cardioprotection against IRI[42]. Overexpression of SA3K in mouse FBs, or SA3 in adult human FBs, resulted in significant upregulation of p-AKT and p-ERK signals in CMs in the corresponding species (Fig. 7a–d). On the contrary, SA3K silencing markedly suppressed AKT and ERK1/2 phosphorylation in mouse CMs (Fig. 7a, b). Similar trends were observed in human cells, but only p-ERK in shSA3#1 reached statistical significance (Fig. 7c, d). The SAFE pathway involves the activation of Janus kinase (JAK) and signal transducer and activator of transcription 3 (STAT-3)[41,43–45], and has been demonstrated to play a key role in I/R protection in mice[46], pigs[47], and humans[48,49]. Overexpression of SA3K in mouse FBs significantly increased JAK2 and STAT3 phosphorylation in N·H·stimulated CMs (Fig. 7e, f). Conversely, the depletion of SA3K resulted in opposing trends. Similar observations were made using adult human cells, marked by significant upregulation of p-STAT3 upon SA3 overexpression, and suppression of STAT3 phosphorylation upon SA3 depletion with shSA3#2 (Fig. 7g, h). Together, these data demonstrate that WNT signaling inhibition and activation of RISK and SAFE cardioprotective pathways by SA3K are critical to CM survival during IRI.

Discussion

Protein lactylation is a newly discovered form of post-translational modification[15], and has since gained particular attention in disease conditions with metabolic reprogramming towards glycolysis, including cancer and myocardial ischemia[10–14]. The accumulation of lactate in ischemic tissue has established its reputation as deleterious waste product[50]. In patients with ST-segment elevation myocardial infarction (STEMI), increased lactate level is correlated with worse prognosis[51,52]. At the molecular level, lactate promoted *Snail1* lactylation to induce TGF-β-mediated endothelial-to-mesenchymal transition[14]. However, this classic view has been challenged due to emerging roles of lactate as a circulating carbohydrate energy source[50] and a signaling molecule[53,54]. Postconditioning with lactate-enriched blood was shown to prevent reperfusion-induced arrhythmia in STEMI patients undergoing reperfusion therapy[54]. Consistent with this view, histone lactylation triggered activation of the reparative transcriptional response (including genes *Lrg1*, *Vegf-a*, and *IL-10*) in monocytes to improve cardiac function post-MI[11]. In a swine model of I/R injury, increased lactate levels promoted the synthetic vascular smooth muscle cell phenotype, which participates in myocardial repair through the upregulated expression of Yes-associated protein (Yap), mechanistic target of rapamycin (mTOR) and adenosine monophosphate-activated protein kinase (AMPK)[55]. Our work unveiled a previously unrecognized role of lactate in enhancing SA3K protein stability through K351la, which protected CMs from I/R-induced apoptosis, shedding light on one of the beneficial consequences of protein lactylation. It therefore appears that the function

of lactate is highly complex, and effectively harnessing the positive downstream functions, while minimizing the detrimental effects, is critical to managing disease outcome.

Cardiac I/R not only causes direct damage to CMs, but also has a serious impact on the cardiac microenvironment[56]. Supporting cells in the cardiac microenvironment (e.g., endothelial cells, immune cells, and fibroblasts) play a vital role in cardiac structural network by the production of extracellular matrix proteins and soluble components to influence cellular communication. In particular, FBs and CMs are known to interact through paracrine and direct cell-to-cell communication during I/R, including transforming growth factor-β (TGF-β), connective tissue growth factor (CNN2/CTGF), angiotensin II (Ang II), cytokines such as interleukin-1 (IL-1) and tumor necrosis factor alpha (TNF-α), and even non-coding RNAs[57]. Most of these factors facilitate tissue damage, promote cardiac remodeling, and impair cardiac function. Our study, however, identified an underappreciated protective role of FBs in I/R through the secretion of lactylated SA3K that suppressed CM apoptosis. Exploring additional constructive roles of FBs during cardiac injury would be necessary for the design of cell type-specific I/R precision therapies, by augmenting their inherent positive functions and blocking their undesirable effects.

Human SERPINA3, also referred to as alpha-1-antichymotrypsin (AACT), is an acute-phase serine protease inhibitor mainly synthesized in the liver, whose major physiological target is neutrophil cathepsin G[58]. A recombinant serine protease inhibitor, LEX032, has been previously shown to attenuate I/R injury by reducing the accumulation of neutrophils in the reperfused myocardium in rats[59]. Another close relative of this protein, mouse Serpina3c, reduced cardiac fibrosis after MI by inhibiting the transcriptional activation of enolase (ENO1), a key enzyme in glycolysis[60]. We showed that SA3K inhibits the WNT pathway and activates RISK and SAFE pathways to prevent CM from undergoing I/R-induced apoptosis, offering insights into critical signaling pathways that control CM survival in I/R. Nonetheless, the physiological and pathophysiological functions of SERPINA3 protein are still only partially understood. The mechanism of modulation of these signaling pathways by SA3K, as well as other biochemical functions of SA3K, remain to be dissected in the future.

Circulating SERPINA3 in humans has served the prognostic stratification of patients with heart failure and MI[34,35], whose cellular origin was previously undetermined. In our study, in addition to confirming FBs as the cardiac source of SA3K in mice and SERPINA3 in humans, we also converted its role from a pure biomarker to a candidate therapeutic approach. Currently, pharmacological and non-pharmacological approaches, alone or in combination, have provided less than desirable advantages in preventing ischemia-induced damage[61]. By contrast, native cardiac proteins have the advantage of little risk of adverse reactions. Based on our data, SA3K lactylation by lactate contributed to the protective effect by enhancing protein stability. Therefore, in a clinical setting, successive doses of SERPINA3 may ameliorate cardiac injury. Alternatively, it would be reasonable to devise a therapeutic strategy using engineered SERPINA3 protein with a slow turnover rate,
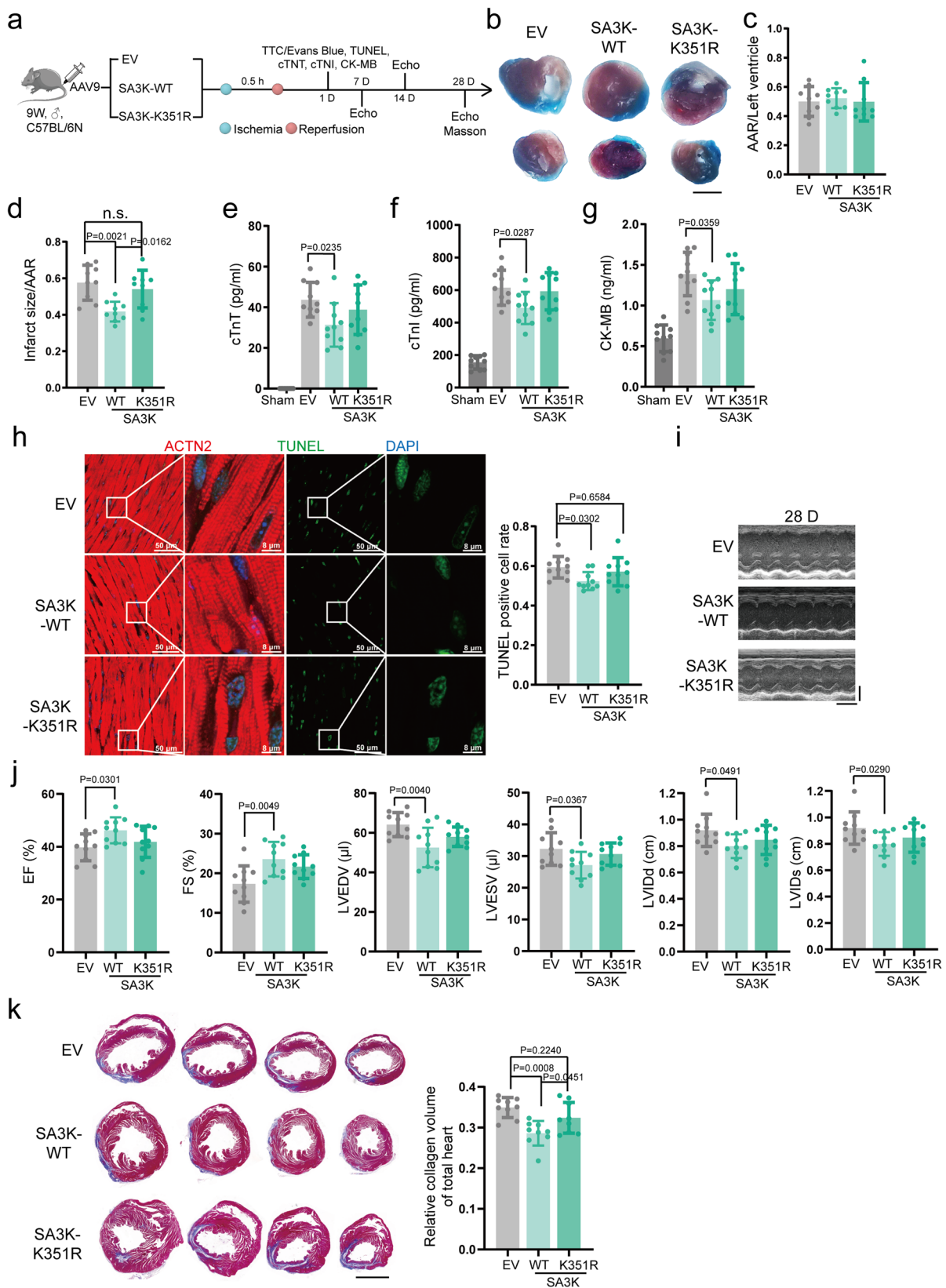
and concurrently reverse increased lactate levels in the I/R-injured heart to minimize other lactate-induced deleterious consequences. In addition, it is also worth exploring whether SERPINA3 and its lactylation play a role in other human cardiac pathologies or in I/R responses of other organs, such as the lung, brain or kidney, such that it can be further exploited for diagnostic or therapeutic purposes.

Methods

Animals

All studies were performed according to the guidelines of the Animal Care and Use Committee, Experimental Animal Center, Fuwai Hospital, National Center for Cardiovascular Diseases, China (0108-7-500-ZX(X)-2). The experiments were reviewed and approved by the Ethics Committee

Fig. 5 | SA3K lactylation at K351 is required for cardiac protection. a Diagram outlining the experimental design for evaluating the role of K351la in I/R. Mice were injected with AAV9 (empty vector (EV), wild-type SA3K (SA3K-WT) and mutant SA3K (SA3K-K351R)) 4 weeks before I/R surgery. Analyses of myocardial ischemia, apoptosis, cardiac function, and fibrosis were performed at indicated time points. **b** Representative photographs showing TTC-stained transverse sections of Evans blue-perfused hearts. **c, d** Area at risk (AAR) (**c**) and infarct size (**d**) were quantified 1 day after IRI, $n = 9$ mice in each group. **e–g** Serum levels of cardiac troponin T (cTnT) (**e**), cardiac troponin I (cTnI) (**f**), and creatine kinase MB (CK-MB) (**g**) were measured 1 day after IRI, $n = 10$ mice in each group. **h** Representative terminal deoxynucleotidyl transferase dUTP nick end labeling (TUNEL) staining images showing apoptotic cell death in heart sections 1 day after IRI. An ACTN2 antibody was used to label cardiomyocytes. Scale bar, 50 μm and

8 μm. Quantification of TUNEL-positive cell rates is shown on the right. $n = 10$ mice in each group, 6 sections per animal. **i** Representative echocardiograms at D28. **j** Quantification of left ventricular ejection fraction (EF), left ventricular fractional shortening (FS), left ventricular end-diastolic volume (LVEDV), left ventricular end-systolic volume (LVESV), left ventricular internal diameter at end diastole (LVIDd), and left ventricular internal diameter at end systole (LVIDs) at D28 based on echocardiography. $n = 10$ mice in each group. **k** Masson's trichrome staining of heart sections 28 days after reperfusion. Scale bar: 2 mm. Quantification of fibrosis is shown on the right. $n = 9$ mice in each group, 4 sections per animal. Significance was calculated using one-way ANOVA followed by Tukey's multiple comparisons test (**d–h, j, k**). All data are means ± SD. Source data are provided as a Source Data file.

---

of Fuwai Hospital, Chinese Academy of Medical Sciences, and Peking Union Medical University. All procedures were performed in compliance with relevant ethical guidelines. Mice were housed under standard laboratory conditions with a 12 h light/dark cycle. Animals were provided with chow (Jiangsu Xietong Pharmaceutical and Bioengineering Co., XTI01WC_009) and water ad libitum. The ambient temperature was maintained at $22 \pm 2\,°C$, with a relative humidity of $50 \pm 10\%$. Mice were randomly assigned to groups by means of drawing lots and the investigators performing the surgeries and cardiac function studies were blinded to mouse genotypes and treatment conditions. For lactylome and proteome analysis, 9- to 13-week-old male wild-type C57BL/6 mice (22 g–25 g) were purchased from Beijing Vital River Laboratory Animal Technology Co., Ltd. Adult female C57BL/6 mice were excluded due to the effect of estrogen on heart ischemia/reperfusion injury[62]. For reproduction, parental adult male and female homozygous SA3K-KO (Cas9) C57BL/6 mice were purchased from GemPharmatech Co., Ltd. Genotyping and reproduction of SA3K-KO mice were carried out at the Experimental Animal Center, Fuwai Hospital, National Center for Cardiovascular Diseases, China. Nine- to 13-week-old offspring male C57BL/6 mice (22 g–25 g) were used in this study. For in vitro cell culture experiments, C57BL/6 neonatal mice (0- to 2-day-old male and female) were purchased from Beijing HFK Bioscience Co., Ltd. The numbers of mice are indicated in corresponding figure legends for each experiment.

Myocardial Ischemia-reperfusion injury model and treatment groups

Mice were anesthetized by intraperitoneal injection of 0.3% pentobarbital sodium. A 20 G catheter was inserted through the larynx into the trachea (endotracheal incubation). Ventilation was performed with a tidal volume of 200 μl, a respiratory rate of 120/min, and 95% oxygen. Throughout the procedure, a self-regulating heating pad was used to maintain their body temperature (36.5–37.5 °C). After disinfection with 2% iodine, the pericardial sac was opened and the left anterior descending artery was temporally occluded with a 7−0 suture. Myocardial ischemia was confirmed by myocardial blanching. After 30 min of ischemia, the suture was released to induce reperfusion injury. An identical procedure was performed in the sham group where a ligature was passed under the left anterior descending without occluding it. After surgery, the chest cavity, muscle and skin were closed, and mice were observed until recovery in a 37.0 °C heated cage. At experimental endpoints, mice were euthanized with an overdose of ketamine (10 mg/ml) and xylazil (1.6 mg/ml). Hearts were perfused with 3–4 ml PBS via intracardiac injection followed by excision of the heart. Hearts were briefly submerged in supersaturated KCl (> 5 M) to arrest the heart in diastole. For experiments evaluating His-SA3K function, mice were injected with recombinant His-SA3K (0.5 mg/kg, Sino Biological CO., LTD, MB16MA1608). His-SA3K was dissolved in a saline solution at a concentration of 0.05 μg/μl and injected via tail vein at the time of reperfusion. For mice in the vehicle control group, an equal volume of saline solution was injected in parallel. For SA3K overexpression experiments,

adeno-associated virus serotype 9 (AAV9) empty vector (AAV9-EV), or AAV9 expressing wild-type or mutant SA3K (AAV9-SA3K-WT and AAV9-SA3K-K351R) were purchased from Vigene Biosciences (Jinan, China) for mouse tail intravenous injection. Each mouse was injected with 5×10^{11} vg/ml (virus gene copy/ml) AAV9 diluted in 200 μl saline solution. Four weeks after AAV9 injection, mice were subjected to I/R surgery.

Echocardiography and hemodynamic analysis

Transthoracic ultrasonography was performed with the Vevo 2100 system (Fujifilm VisualSonics, Ontario, Canada). Echocardiography and hemodynamic analysis were performed before I/R surgery and at days 7, 14, and 28 after I/R surgery. Mice were anesthetized by inhalational flow of isoflurane, while maintaining their heart rate at 450–550 beats/min. The peak aortic blood velocity across the aortic constriction was measured in the pulsed wave color doppler mode. Left ventricular function was assessed by M-mode scanning of the left ventricular chamber, and standardized by two-dimensional, short axis views of the left ventricle at the mid papillary muscle level. Left ventricular chamber size and wall thickness were measured for at least three beats from each projection and averaged.

Protein preprocessing for LC-MS/MS

Twenty seven mice from Sham, MI and I/R groups (3 biological replicates in Sham, MI, I/R, respectively; 3 cardiac samples were combined as one biological replicate) were collected for proteome/lactylome analysis, respectively. Left ventricular samples were collected in liquid nitrogen and grinded into powder. Further sonication of the tissue fragments was performed on ice in a urea-containing lysis buffer (8 M urea, 1% protease inhibitor cocktail, 3 μM trichostatin A (TSA), 50 mM N-acetylmuramic acid (NAM) and 2 mM EDTA) using a high-intensity ultrasonic processor (Xiaomei Ultrasonic Instrument (Kunshan) Co., Ltd., XM-26A). Lysed tissue was centrifuged at $12,000 \times g$ at 4 °C for 10 min, and the supernatant was collected. Protein concentration was determined using a BCA kit according to the manufacturer's instructions (P0011, Beyotime, China).

Equal amounts of protein were retrieved from each sample, and the final volume was adjusted using the lysis buffer to ensure equal concentration. Trichloroacetic acid (TCA) was slowly added to a final concentration of 20% and briefly vortexed for precipitation at 4 °C for 2 h. The sample was then centrifuged at $4500 \times g$ for 5 min, and the supernatant was discarded. The precipitate was rinsed with precooled acetone. After air drying, tetraethylammonium bromide (TEAB) was added to a final concentration of 200 mM. Then, the precipitate was sonicated. Trypsin was added at a ratio of 1: 50 (trypsin: protein, m/m), and the sample was digested at 37 °C overnight. Dithiothreitol (DTT) was added into the solution at a final concentration of 5 mM for reduction at 56 °C for 30 min. Iodoacetamide (IAM) was finally added to a final concentration of 11 mM to alklyate reduced cysteine residues. The sample was incubated at room temperature for 15 min, protected from light.
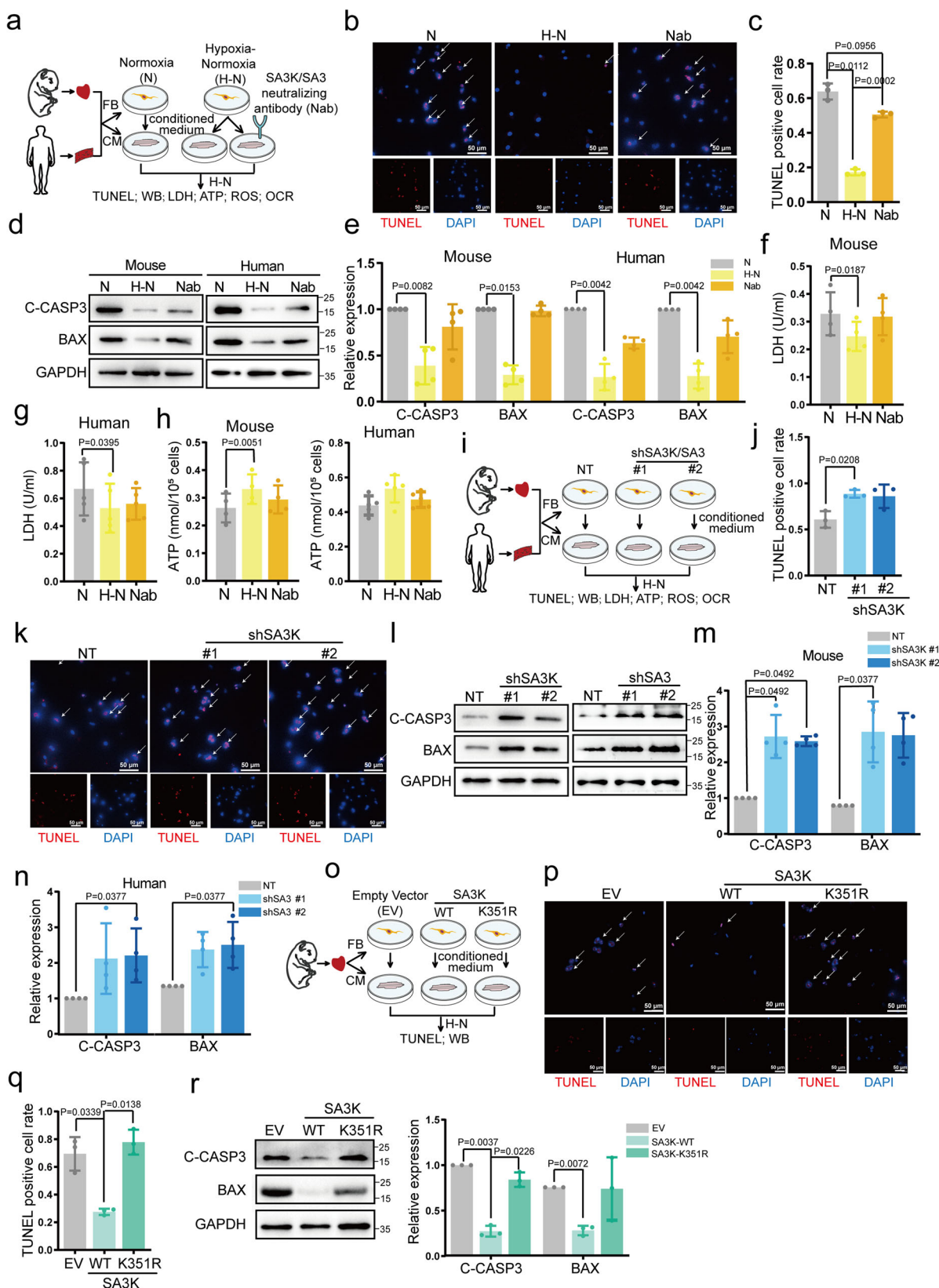
Enrichment of lactylated peptides

To enrich for lactylated peptides, digested peptides dissolved in NETN buffer (100 mM NaCl, 1 mM EDTA, 50 mM Tris-HCl, 0.5% NP-40, pH 8.0) were incubated with pre-washed pan-lactylation antibody beads (PTM Bio, PTM-1404) at 4 °C overnight with gentle shaking. Then, the beads were washed for four times with NETN buffer and twice with water. Bound peptides were eluted from the beads with 0.1% trifluoroacetic acid. Finally, the eluted fractions were combined and vacuum dried. For LC-MS/MS analysis, the resulting peptides were desalted with C18 ZipTips (Millipore, ZTC18M096) according to the manufacturer's instructions.

Fig. 6 | SA3K/SA3 secreted by FBs protect CMs from IRI-induced apoptosis through paracrine signaling. a Experimental design. Cardiac FBs from neonatal mice or adult humans were cultured under normoxia (N) or hypoxia-normoxia (H-N) conditions. CMs were treated with conditioned media, and subjected to H-N. Nab, neutralizing antibody. **b** TUNEL staining of apoptotic cells (white arrow). Scale bar, 50 µm. **c** Quantification of (**b**). $n = 3$ independent experiments. **d** Western blotting of cleaved caspase 3 (C-CASP3) and BAX in neonatal mouse and adult human CMs. **e** Quantification of (**d**). $n = 4$ independent experiments. **f, g** Quantification of LDH in mouse (**f**) or human (**g**) CM supernatant. $n = 4$ (mouse) or 5 (human) independent experiments. **h** Quantification of cellular ATP concentration in mouse (left) or human (right) CMs. $n = 4$ (mouse) or 5 (human) independent experiments. **i** Experimental design. SA3K and SA3 were silenced by shRNA in neonatal mouse and adult human FBs, respectively. Corresponding CMs were treated with conditioned media, and subjected to H-N. **j, k** Quantification of TUNEL-positive cells (**j**), and representative images of TUNEL staining (**k**). White arrows indicate TUNEL-positive cells. Scale bar, 50 µm. $n = 3$ independent experiments. **l** Western blotting of C-CASP3 and BAX in neonatal mouse and adult human CMs. **m, n** Quantification of (**l**) (**m**, mouse; **n**, human). $n = 4$ independent experiments. **o** Experimental design. Neonatal mouse FBs were transduced with lentivirus expressing empty vector (EV), SA3K-WT or SA3K-K351R. Neonatal CMs were treated with conditioned media, and subjected to H-N. **p, q** TUNEL staining (**p**) and quantification (**q**) of apoptotic CMs. White arrows indicate TUNEL-positive cells. Scale bar, 50 µm. $n = 3$ independent experiments. **r** Western blotting of C-CASP3 and BAX in neonatal mouse CMs. Quantification is shown on the right. $n = 3$ independent experiments. Significance was calculated by repeated-measures one-way ANOVA followed by Tukey's multiple comparisons (**c, f–h, j, q**), or by the Kruskal-Wallis test followed by Dunn's multiple comparisons test (**e, m, p, r**). GAPDH loading control was run on a separate gel in (**l, r**). All data are means ± SD. Source data are provided as a Source Data file.

LC-MS/MS analysis

For proteomic profiling, we used a four-dimensional (4D) label-free quantification approach (Fig. 1a). 4D proteomics integrates a fourth dimension, i.e., ion mobility, into the 3 dimensions of classic proteomics, improving peptide and protein identification[22]. Tryptic peptides were dissolved in solvent A (0.1% formic acid, 2% acetonitrile in water). Then, peptides were separated using a nanoElute ultra-high-performance liquid chromatography (UHPLC) system (Bruker Daltonics, Inc., Billerica, MA, USA). Solvent B was 0.1 % formic acid in acetonitrile. All steps were performed at a constant flow rate of 450 nl/min, with liquid level gradient setting: 0–42 min, 7–24% B; 42–54 min, 24–32% B; 54–57 min, 32–80% B; 57–60 min, 80% B. After separation by UHPLC system, 40 µg of peptides per sample were loaded onto a capillary column for ionizatoin. Samples were analyzed by the timsTOF Pro mass spectrometer (Bruker Daltonics). The electrospray voltage applied was 1.60 kV. Precursor and fragment ions were analyzed at the time-of-flight (TOF) detector, with an MS/MS scan range of 100–1700 m/z. The timsTOF Pro was operated in parallel accumulation-serial fragmentation (PASEF) mode. Precursor ions with charge states of 0–5 were selected for fragmentation, and 10 PASEF-MS/MS scans were acquired per cycle. The dynamic exclusion setting was 30 s.

Database search

MS/MS data were processed using the MaxQuant search engine (v.1.6.15.0). Tandem mass spectra were searched against the human SwissProt database (20,422 entries) concatenated with reverse decoy database. Trypsin/P was specified as cleavage enzyme allowing up to 2 missing cleavages. The mass tolerance for precursor ions was set as 20 ppm in the first search and 5 ppm in the main search, and the mass tolerance for fragment ions was set as 0.02 Da. Carbamidomethyl on Cys (average mass 57.0513) was specified as fixed modification, and acetylation on protein N-terminus (average mass 42.0367), oxidation on Met (average mass 15.9994), and lactylation on lysine (average mass 72.021) were specified as variable modifications. The false discovery rate (FDR) was adjusted to < 1%.

Data normalization

Raw LC-MS datasets were first searched against the database and converted into matrices containing intensity of peptides across samples. The relative quantitative value of each peptide was then calculated based on these intensity data by the following steps:

Firstly, the intensities of peptides (I) were centralized and transformed into relative quantitative values (R) of peptides in each sample. The formula is listed as follow: i denotes the sample and j denotes the peptide.

$$R_{ij} = I_{ij} / Mean(I_j) \tag{1}$$

For normalization of Kla modifications, the relative quantitative value of the modified peptide (from lactylome) was divided by the relative quantitative value of corresponding protein (from proteome) to remove the influence from protein expression on modifications.

Motif analysis

We applied the MoMo software tool, which fully re-implements motif-x and MoDL[29], to analyze and extract overrepresented motifs from Kla-21-mers (10 amino acids upstream and downstream of the site) in all protein sequences[63]. The minimal number of peptide occurring in one motif "occurrences" was set to 20, and the motif analysis statistics test significance threshold value was set to 0.0000001 (Fisher's exact test). The heatmap of amino acids frequencies occurring near lactylation sites (Difference Score, DS, Supplementary Fig. 1h) was calculated using the following equation:

$$DS = -Log10(p.value) * sign(diff.percent) \tag{2}$$

We also used iceLogo to examine the properties of amino acids surrounding the modification sites using t-test. A P-value < 0.05 was considered statistically significant[64].

Secondary structure prediction

The secondary structures and surface accessibility was analyzed using NetSurfP1.0 software including alpha-helix, beta-strand and coil. For specific amino acid positions, the average probability and surface accessibility of the three secondary structures with and without modification were calculated respectively. P values were calculated by Wilcoxon rank sum test.

Density gradient

The density gradient was analyzed using R package "ggplot2" software. Log 2 ratios of fold changes of proteins and modification sites were visualized by "geom_density" as density gradient (cutoff of $|Log_2FC| > 1.0$).

Differential analysis

Firstly, the samples to be compared pairwise were selected, and the fold change (FC) was calculated as the ratio of the mean intensity for each modification site in two sample groups. For example, to calculate the fold change between sample A and sample B, we used the following equation:

$$FC_{A/B, k} = Mean(R_{ik}, i \in A) / Mean(R_{ik}, i \in B) \tag{3}$$

R denotes the relative quantitative value of the modification site, i denotes the sample and k denotes the modification site.
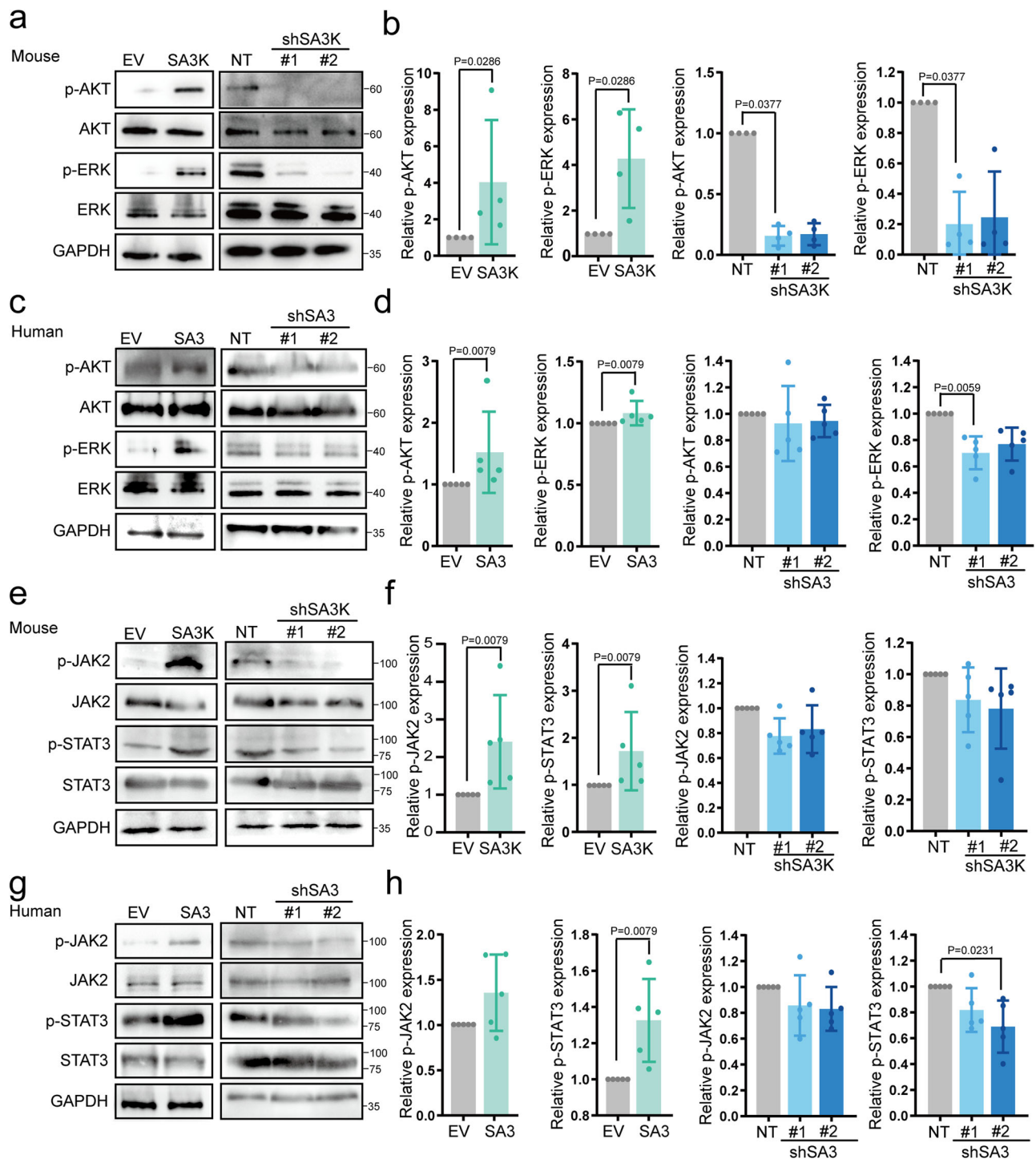
Fig. 7 | SA3K/SA3 protect CMs by inhibiting the WNT pathway and activating cardioprotective RISK and SAFE pathways. a–d Western blots (**a**, **c**) and quantification (**b**, **d**) of p-AKT, AKT, p-ERK, and ERK in neonatal mouse (**a**, **b**) and adult human CMs (**c**, **d**) treated with conditioned media from FBs with SA3K/SA3 overexpression or depletion. GAPDH was used as loading control. *n* = 4 (**b**) or 5 (**d**) independent experiments. **e–h** Western blots (**e**, **g**) and quantification (**f**, **h**) of p-JAK2, JAK2, p-STAT3 (Tyr705), and STAT3 in neonatal mouse (**e**, **f**) and adult

human CMs (**g**, **h**) treated with conditioned media from FBs with SA3K/SA3 overexpression or depletion. GAPDH was used as loading control. *n* = 5 independent experiments. All overexpression data were analyzed using the two-tailed Mann-Whitney test, while all knockdown data were analyzed using the Kruskal-Wallis test followed by Dunn's multiple comparisons. For (**a**, **c**, **g**), GAPDH loading control was run on a separate gel. Data are means ± SD. Source data are provided as a Source Data file.

To calculate the significance of the difference between groups, Student's *t*-test was performed on the relative quantitative value of each modification site in the two sample groups, and the corresponding *P*-value was calculated as the significance index. A *P*-value of < 0.05 was considered as significant. To make

the data conform a normal distribution, the relative quantitative value of modification site was log2 transformed using the following equation:

$$P^k = \text{T.test}(\text{Log2}(R_{ik}, i \in A), \text{Log2}(R_{ik}, i \in B)) \tag{4}$$

Modification sites with *P* value < 0.05 and *FC* > 1.3 were considered significantly up-regulated sites, while the modification sites with *P*-value < 0.05 and *FC* < 1/1.3 were regarded as significantly down-regulated sites[65]. For protein expression changes (proteome), a cutoff of $|Log_2FC| > 1.5$ was imposed.

Clustering of differentially lactylated or expressed proteins and GO analysis

Differentially expressed proteins were clustered according to their expression patterns through the sampling series by hclust and cutree functions in R[66]. Further, the mean with confidence interval of a standard *t*-test of proteins is plotted over groups to show the expression patterns of each cluster. For each cluster of proteins, GO enrichment analysis was conducted by clusterProfiler (v3.2.14)[67].

Gene Ontology (GO) annotation was derived from the UniProt-GOA database (http://www.ebi.ac.uk/GOA/). Identified protein IDs were first converted to UniProt IDs, and then mapped to GO IDs. In cases where identified proteins were not annotated in the UniProt-GOA database, the InterProScan was used to annotate the proteins' GO functions based on protein sequence alignment results. Proteins were annotated based on two sub-ontologies, i.e., biological process (Fig. 1g, i) and molecular function[68,69] (Supplementary Fig. 2c).

Functional annotation network

All differentially expressed proteins were searched against the STRING database (version 11.0) for functional and physical protein-protein interactions (full STRING network, where edges indicate both functional and physical protein associations). Protein interaction relationships with a confidence score > 0.4 (medium confidence) were extracted. Interaction networks from STRING were visualized using R package "networkD3"[70].

Neonatal mouse primary cardiomyocytes and fibroblasts

Neonatal mouse cardiomyocytes and neonatal mouse fibroblasts were isolated from C57BL/6 1- to 2-day-old neonatal mouse hearts. Hearts were transferred to PBS containing heparin sodium (1000 units in 50 ml PBS) for washing, and then chopped into small pieces and digested with the Pierce™ Primary Cardiomyocyte Isolation Kit (Thermo, 88281) according to the manufacturer's instructions. To obtain relatively pure cardiomyocytes, we used the differential velocity adherence method to culture isolated cells for 1 h. Non-adherent cells were collected as cardiomyocytes, and were cultured in DMEM containing 10% FBS and 1% penicillin-streptomycin (P/S) on 0.1% gelatin (2×10^5 cells per well in 6 well-plates). Neonatal mouse fibroblasts were plated at 1×10^6 cells per well in 6 cm plates and cultured in DMEM containing 10% FBS and 1% P/S.

Adult human primary cardiomyocytes and fibroblasts

The study was approved by the Ethics Committee of Fuwai Hospital, Chinese Academy of Medical Sciences, and Peking Union Medical University, and conducted according to the Declaration of Helsinki (2021-1533). Written informed consent was obtained from all patients. Patient information is listed in Supplementary Table S4. of the Supplementary information.

The isolation and culture of human primary CMs were performed as previously described[71]. In brief, cardiac specimens were cut into tissue slices (300 μm), chopped and transferred to a Tyrode solution (126 mM NaCl, 4.4 mM KCl, 5 mM MgCl₂·6H₂O, 5 mM NaH₂PO₄, 5 mM HEPES, 22 mM glucose, 20 mM taurine, 5 mM creatine, 5 mM sodium pyruvate, supplemented with 10 μM (-)-blebbistatin (Selleck, S7099), 250 U/ml Type II collagenase and 1.2 U/ml protease XXIV (Sigma, P8038) for digestion. After 50 min in a 37 °C bath shaker, the tissue was transferred to a fresh digestive solution that does not contain proteases for further digestion. Rod-shaped CMs were collected by centrifugation ($100 \times g$, 3 min, 4 °C). Calcium concentration was gradually restored to 1.8 mM prior to culture in MEM (HEPES, GlutaMAX™, Gibco, 42360099) supplemented with 10% FBS (Gibco), 100 U/ml P/S (Gibco, 15140163), 100 μg/ml Primocin (InvivoGen, ant-pm-05) and 10 μM (-)-blebbistatin.

The isolation and culture of human primary FBs were performed as previously described[71]. FBs were isolated by digesting myocardial tissue fragments in a solution containing 2 mg/ml Collagenase I (Worthington, LS004196), 2 mg/ml Collagenase II (Worthington, LS004176), and 0.1% BSA dissolved in DMEM-F12 (Gibco, 11330-032) supplemented with 1% P/S. After 25 min in a 37 °C bath shaker, the cell suspension was filtered through a 40 μm filter. After incubation in red blood cell lysis buffer (Thermo, 00-4333-57) for 4 min, an equal volume of PBS containing 10% FBS was added for neutralization. FBs were centrifuged at $300 \times g$, 3 min, 4 °C, resuspended in DMEM-F12 supplemented with 20% FBS and 1% P/S, and then plated into 6-well plates (0.1% gelatin-coated) for culture.

Hypoxia treatment

Hypoxia (24 h) of cell cultures was achieved using a Heracell™ VIOS 160i incubator (Thermo Fisher Scientific Madison, WI, USA) filled with 94% N_2, 5% CO_2, and 1% O_2. Reoxygenation was performed by transferring the culture to a normoxic incubator with 5% CO_2 and 95% air. Neutralized antibody treatment was performed by adding SA3K (Proteintech, 55480-1-AP) or SERPINA3 (Abcam, ab205198) antibodies directly into conditioned media at a concentration of 1 μg/ml and incubated at room temperature for 4 h, before transfer to CM cultures.

Western blotting

Protein was harvested from cultured cells by lysis using RIPA buffer (10 mM Tris-Cl pH 8.0, 1 mM EDTA, 0.5 mM EGTA, 1% Triton X-100, 0.1% sodium deoxycholate, 0.1% SDS and 140 mM NaCl) supplemented with 1× protease and phosphatase inhibitor cocktail (Thermo, 78445). After centrifugation at 4 °C, $14,000 \times g$, 15 min, cellular supernatants was boiled in 5 × sample buffer (250 mM Tris-HCl (pH 6.8), 8% (w/v) sodium dodecyl sulfate (SDS), 0.2% (w/v) bromophenol blue, 0.3 M DDT, 30% (v/v) glycerol, 10% (v/v) β-mercaptoethanol). Protein concentration was determined by BCA Protein Assay (Beyotime, P00125). Equal amounts of proteins were separated via SDS-PAGE and electrotransferred onto a PVDF membrane (Millipore, IPVH00010). Membranes were then blocked with 5% skim milk in TBST and incubated with primary antibodies at 4 °C overnight. Antibody dilutions are shown in Supplementary Table S3. After 3 washes with TBST, membranes were incubated with corresponding secondary antibodies diluted in blocking buffer for 1 h at room temperature. Secondary antibodies included anti-rabbit IgG, HRP-linked antibody (Cell Signaling, 7074S) and anti-mouse IgG, HRP-linked antibody (Cell Signaling, 7076S), which were used at a 1:5000 dilution ratio. Blots were developed using the Clarity™ Western ECL Substrate (Bio-Rad, 1705060) on the Tanon 5800 Multi (Tanon, Shanghai, China) Chemi-Image System according to the manufacturer's instructions. Densitometric analyses were performed using ImageJ v1.42q.

Immunoprecipitation

Cells were lysed using a lysis buffer containing 20 mM Tris-HCl pH 7.5, 150 mM NaCl, 1 mM EDTA, 1% nonidet P-40, 0.5% sodium deoxycholate and 0.1% SDS, supplemented with 1× protease inhibitor cocktail (Roche, 4693132001). After centrifugation (4 °C, $14000 \times g$, 15 min) cellular supernatants was transferred to a new tube and incubated with protein A/G agarose beads (Yeasen, 36417ES03) for 2 h at 4 °C. The precleaned lysates were incubated with anti−pan-Kla, anti-pan-Kac or rabbit IgG overnight at 4 °C, and further incubated with 20 μl of protein A/G agarose beads for 4 h at 4 °C. Finally, precipitates were washed with lysis buffer and boiled in 5 × sample buffer (250 mM Tris-HCl (pH 6.8), 8% (w/v) sodium dodecyl sulfate (SDS), 0.2% (w/v) bromophenol

blue, 0.3 M DDT, 30% (v/v) glycerol, 10% (v/v) β-mercaptoethanol). Samples were subjected to Western blotting with an SA3K antibody.

Generation of the polyclonal rabbit anti-SA3K-K351la antibody

The polyclonal rabbit anti-SA3K-K351la antibody was raised using against two synthetic SA3K peptides with K351-Kla (ITETK-(lactyl)K-LSVSQ and SGITETK-(lactyl)K-LSVSQ) to trigger immune responses in pathogen-free barrier facility-raised New Zealand White rabbits (PTM Biolab Co., Ltd.). A nonlactylated peptide (SGITETKKLSVSQ) was also generated and verified by MS analysis. After immunization, sera were purified using protein A and collected for quality control (dot blot analysis).

Dot blot analysis

Four modified or unmodified SA3K peptides were synthesized by PTM Biolab Co., Ltd.

The peptide sequences were as follows:
SA3K-Kla-1: CITETK-(lactyl)K- LSVSQ
SA3K-Kla-1: CSGITETK -(lactyl)K- LSVSQ
SA3K-Ksucc: CSGITETK-(succinyl)K- LSVSQ
SA3K: CSGITETKKLSVSQ

Peptides (1 ng, 4 ng, 16 ng, 64 ng) from each group were blotted onto a PVDF membrane. After drying, the PVDF membrane was incubated in blocking buffer for 1 h, and then with the anti-SA3K-K351la (Ab-Kla-1) primary antibody solution (diluted 1:1000 in blocking solution) for 2 h at room temperature. After washing the membrane in washing buffer 3 times, an HRP-linked anti-rabbit IgG secondary antibody (Cell Signaling, 7074S) was used at a 1:5000 dilution ratio. After washing the membrane in washing buffer (3×10 min), blots were developed using the Immobilon™ Western Western Chemiluminescent HRP Substrate (Millipore WBKLS0500), and imaged on the Tanon 5200 Multi (Tanon, Shanghai, China) Chemi-Image System.

Enzyme-Linked Immunosorbent Assay (ELISA)

The medium concentration of SERPINA3 was examined via ELISA assay according the manufacturer's instructions (Abcam, ab217779). In brief, 50 μl medium or standard samples were added to wells in a 96-well plate. Then, 50 μl of antibody cocktail was added to each sample, followed by incubation at room temperature for 1 h. Each well was washed three times with 350 μl 1× wash buffer. TMB development solution (100 μl) was added to each well and incubated for 10 min, followed by the addition of 100 μl stop solution. OD values were measured at 450 nm on a microplate reader (Tecan, Infinite-M200).

For the measurement of cardiac injury markers in the serum of mice, mouse blood was collected from the abdominal aorta. Mice were fully anesthetized using isoflurane inhalation, followed by insertion the needle of a 1 ml syringe into the abdominal aorta. The serum concentration of CK-MB was examined using an ELISA assay (Songon, D721065) according to the manufacturer's instructions. In brief, serum samples were diluted 1:4 using a dilution buffer, after which 100 μl of the diluted serum or standard samples were added into 3 replicate wells per sample in 96-well plates. After incubation at 37 °C for 90 min, 100 μl biotin-CK-MB was added to the 96-well plate and incubated at 37 °C for 60 min. Each well was washed 4 times with 350 μl washing buffer. Then, 100 μl of HRP working buffer was added to the 96-well plate, and incubated at 37 °C for 30 min. After washing 4 times with 350 μl of washing buffer, 90 μl substrate solution was added, and further incubated at 37 °C for 15 min. Finally, 50 μl stop solution was added to each well. OD values were measured at 450 nm on a microplate reader (Antobio, Phomo).

The serum concentrations of cTnT and cTnI were examined using ELISA assay kits (Cloud-clone corp, SEA820Mu and SEA478Mu) according the manufacturer's instructions. In brief, 100 μl of diluted serum (described above) or standard samples were added to wells in a 96-well plate, followed by incubation at 37 °C for 1 h. After aspiration, 100 μl detection reagent was added to each sample, followed by incubation at 37 °C for 1 h. Each well was washed three times using washing buffer. Substrate solution (90 μl) was added to each well and incubated at 37 °C for 20 min, followed by the addition of 50 μl stop solution. OD values were measured at 450 nm on a microplate reader (Antobio, Phomo).

ROS detection

Neonatal mouse cardiomyocytes and adult human primary cardiomyocytes were seeded into black 96-well cell culture plates (Corning, 3904) and treated with hypoxia and normoxia. To quantify cell ROS production, cardiomyocytes were incubated with 5 μM of CellROX (Thermo, C10444) in PBS for 30 min at 37 °C according to the manufacturer's instructions. Next, cardiomyocytes were washed with PBS 3 times and fluorescence intensity was measured at 485/520 on a microplate reader (Antobio, Phomo).

Measurement of ATP concentration

Neonatal mouse cardiomyocytes and adult human primary cardiomyocytes were seeded into white 96-well cell culture plates (Corning, 3606) and treated with normoxia or hypoxia-normoxia. Cellular ATP concentrations were assessed using the CellTiter-Glo® Luminescent Cell Viability Assay (Promega, G8461) per manufacturer's instructions. In brief, 1 μM ATP (Sigma, P1132) diluted with culture medium into serial tenfold solutions (100 μl contains 10^{-10} to 10^{-13} moles of ATP) were added into white 96-well plates for plotting the standard curve. Then, 100 μl CellTiter-Glo® Reagent was add to standard wells and wells containing cells. After mixing the contents for 2 min on an orbital shaker, the plate was incubated at room temperature for 10 min to stabilize the luminescent signal. Luminescence intensity was measured using a microplate reader (Antobio, Phomo).

LDH measurement

LDH was measured using the LDH-Glo™ Cytotoxicity Assay kit (Promega, J2380) according to the manufacturer's instructions. Cellular supernatant was diluted 1:100 in culture medium. Standard samples and cellular supernatant were added in triplicate into white 96-well plates (50 μl/well). The LDH detection reagent was added at a 1:1 (v/v) ratio into the wells. The reaction was incubated in the dark for 1 h at room temperature, before luminescence values were measured using a plate reader (Antobio, Phomo).

Masson's trichrome staining

To analyze tissue fibrosis, mice were euthanized at 28 D post I/R. The infarcted areas of mouse heart tissues were sectioned at 4 μm for 10 serial sections per short axis view, and continued at intervals of 400 μm from the ligation site to the apex. A total of five short axis section levels were obtained for each heart. Histochemical staining was performed as previously described[72]. In brief, histological analyses were performed on heart tissues that were fixed in 4% paraformalin at room temperature for 48 h and embedded in paraffin. Masson's trichome staining was performed on representative sections of each short axis level to evaluate collagen deposition. Masson's staining (Leagene, DC0033) was performed according to the manufacturer's protocol. Histopathological images were acquired with Pannoramic SCAN (3Dhistech, Hungary). Fibrotic area and total heart area were calculated through the combined analysis of sections from 4 short axis levels, excluding the one closest to the ligature. The relative collagen volume (fibrotic area/ total heart area) for each heart is the averaged value of all four levels.

Immunofluorescence

For immunofluorescence analyses, heart sections were incubated with primary antibodies (1:50 dilution), including anti-SA3K, anti-ACTN2

and anti-VIMENTIN antibodies, at 4 °C overnight. Then, secondary antibodies, including goat anti-rabbit-Alexa Fluor 488 (Thermo, A32731, 1:1000 dilution) or goat anti-mouse-Alexa Fluor 594 (Thermo, A11032, 1:1000 dilution) antibodies, were applied for 2 h at room temperature in the dark. Sections were mounted with DAPI (Thermo, P36981). Sections were viewed on a Leica SP8 confocal microscope (Leica Microsystems, Germany), using a 40× water immersion objective or 60 × oil immersion objective, with identical exposure times. Images were further magnified by electronic magnification when necessary. Quantification of immunofluorescence staining was performed using the image analysis software ImageJ 1.42q. Specifically, the integrated optical density (IOD) was obtained by summing all optical density values of each channel within an image. Mean densities were calculated by dividing IOD by the distribution area of the target of interest.

Measurement of infarct size and area at risk

At 24 h post I/R, the LAD was re-occluded, and 2% Evans blue dye (Sigma, E2129) was injected into the heart cavity through the ascending aorta. After euthanization, hearts were frozen at −80 °C for 30 min, and the myocardium below the ligature point was cut into four 2 mm-thick slices. The slices were incubated with 2 % 2,3,5-triphenyltetrazolium chloride (TTC, Sigma, T8877) at 37 °C for 10 min in a dark room and then fixed in 4 % formalin for 2 h. Following staining, the slices were imaged with a digital camera (SONY Alpha 6400 APS-C, SELP1650). The infarcted area was not stained by TTC. The area at risk was identified by the lack of blue dye. The infarcted tissue was measured and calculated using ImageJ v1.42q.

Terminal deoxynucleotidyl transferase dUTP nick end labeling (TUNEL) staining

To assess cell death in I/R heart tissues, the TUNEL assay was performed on heart sections using the In-Situ Cell Death Detection Kit (Roche, 11684817910) according to the manufacturer's instructions. Meanwhile, anti-ACTN2 primary antibody was used to detect CMs. Nuclei were visualized by DAPI. Two images from infarct, border, and remotes zones, respectively, from sections at the plane right below the ligation spot were chosen for quantification. Sections were imaged on a confocal laser scanning microscope (Leica SP8, Germany) using a 60× oil immersion objective. TUNEL-positive cells that displayed colocalization with DAPI were counted as apoptotic cells (Figs. 4h and 5h), while TUNEL colocalization with and ACTN2 (Supplementary Fig. 9a and 9b) were considered apoptotic CMs.

To investigate cell death in primary cardiomyocytes, neonatal mouse CMs were plated into 15 mm confocal dishes for immunofluorescence staining. After culturing, CMs were fixed with 4% paraformaldehyde for 7 min, and permeabilized in 0.1% Triton X-100 for 7 min. Then, TUNEL assay was performed using the TUNEL Cell Apoptosis Detection Kit (KeyGEN, KGA7062) according to the manufacturer's instructions. Finally, CMs were mounted with DAPI (Thermo, P36981). CMs were imaged on a confocal laser scanning microscope (Leica SP8, Germany) using a 40× water immersion objective. TUNEL-positive cells that displayed colocalization with DAPI were counted.

L-lactate measurement

L-lactate levels were measured by a Lactate Assay Kit (Elabscience, E-BC-K044-M) according to the manufacturer's protocol. In brief, to prepare cell samples, 1×10^6 cells were homogenized in 300 µl PBS. To prepare tissue samples, 1 g heart tissue was homogenized in 9 ml PBS, followed by centrifugation at $10,000 \times g$ for 10 min. Five microliters of samples or standards were added into each well with 100 µl enzyme working solution. After incubation for 10 min at 37 °C, OD values of each well were measured at 530 nm on a microplate reader (Tecan, Infinite-M200).

Plasmids, transfection, lentivirus production and infection

Mouse SA3K-WT and SAK-K351R cDNAs were subcloned into the pHBLV-CMV-MCS-3flag-EF1-puro vector to generate the FLAG-tagged plasmids. shRNAs for the target genes were cloned into the pHBLV-U6-MCS-PGK-PURO vector. The sequences for shRNAs were as follows:

sh-SA3K#1: AGTCTGAGTTCTACTTGGATGAGAA;
sh-SA3K#2: CAGGAAATGCCAGCGCCCTGTTTAT.

All plasmids were purchased from Hanbio Co. Ltd, Shanghai, China. Lentivirus was packaged using 293T cells. Briefly, lentiviral pHBLV-shRNA-Puro plasmids, and psPAX2 and pMDLg/pRRE plasmids, were transfected into 293 T by Lipofectamine™ 3000 (Thermo, L3000008). Virus-containing supernatants were collected at 48 and 72 h after transfection and centrifuged at $1200 \times g$ for 5 min to remove cell debris. For lentivirus infection, viral supernatants were directly transferred to neonatal mouse FBs or CMs, and incubated for 6 h. Polybrene (1 µg/ml) was added to the medium to improve infection efficiency. After infection, cells were cultured continually and used for further analysis.

qRT-PCR

Total RNA was extracted using Trizol (Thermo Fisher Scientific, 15596018) according to the manufacturer's instructions. Reverse transcription was performed using ReverTra Ace® qPCR RT Kit (Toyobo, FSQ-101). Quantitative PCR was performed using SYBR® Green Realtime PCR Master Mix (Toyobo, QPK-201) on an Applied Biosystems 7500 real-time PCR system. The primers used were:

SA3K: 5′-TGAGGAGCTATCGTGCTCTGT-3′ (forward)
5′-GCCTGTAGTTACTAGCGATGGA-3′ (reverse),
SA3: 5′-GTGGTCCATAAGGCTGTGCT-3′ (forward)
5′-GGCCTGTTGAAACGCACAAT -3′ (reverse);
GAPDH 5′-ACGGATTTGGTCGTATTGGG-3′ (forward)
5′-TGATTTTGGAGGGATCTCGC-3′ (reverse).

Protein degradation assays

Determination of protein half-life was performed by treating neonatal mouse FBs with cycloheximide (50 µg/ml, Sigma, C7698). Alternatively, FBs were treated with CHX in presence of a proteasome inhibitor MG132 (20 µM, Sigma, M8699). DMSO was added to untreated control cells. Half-life calculation and visualization were performed by R (4.0.3) and ggplot2 (3.3.2) package.

Statistical analysis

All experiments were repeated for at least 3 biological replicates. Statistical analyses were performed by using GraphPad Prism 8.2.1 (GraphPad Software Inc., La Jolla, CA, USA). For comparisons between two groups of equal sample size, unpaired two-tailed Student's t-test was performed. For multiple comparison testing, a one-way analysis of variance (ANOVA) accompanied by Tukey's post hoc test was used. Paired Student's t-test and repeated-measures one-way ANOVA were used for paired samples. Non-parametric Mann-Whitney (two groups) or Kruskal-Wallis (more than two groups) tests were used for the analysis of data where the control values were normalized to 1. Data were expressed as mean ± SD. Exact P values are indicated within the figures.

Reporting summary

Further information on research design is available in the Nature Portfolio Reporting Summary linked to this article.

Data availability

The authors declare that all data supporting the findings of this study are available within the article and its supplementary information files or from the corresponding author upon reasonable request. The protein mass spectrometry data generated in this study have been

deposited in the PRIDE database under accession code PXD046631. Source data are provided with this paper.

References

1. Zhang, M. et al. Ischemia-reperfusion injury: molecular mechanisms and therapeutic targets. *Signal Transduct. Target. Ther.* **9**, 12 (2024).
2. Ibáñez, B., Heusch, G., Ovize, M. & Van de Werf, F. Evolving therapies for myocardial ischemia/reperfusion injury. *J. Am. Coll. Cardiol.* **65**, 1454–1471 (2015).
3. Fröhlich, G. M., Meier, P., White, S. K., Yellon, D. M. & Hausenloy, D. J. Myocardial reperfusion injury: looking beyond primary PCI. *Eur. Heart J.* **34**, 1714–1722 (2013).
4. Turer, A. T. & Hill, J. A. Pathogenesis of myocardial ischemia-reperfusion injury and rationale for therapy. *Am. J. Cardiol.* **106**, 360–368 (2010).
5. Piot, C. et al. Effect of cyclosporine on reperfusion injury in acute myocardial infarction. *N. Engl. J. Med.* **359**, 473–481 (2008).
6. Ottani, F. et al. Cyclosporine A in Reperfused Myocardial Infarction: The Multicenter, Controlled, Open-Label CYCLE Trial. *J. Am. Coll. Cardiol.* **67**, 365–374 (2016).
7. Thiele, H. et al. Impact of high-dose N-acetylcysteine versus placebo on contrast-induced nephropathy and myocardial reperfusion injury in unselected patients with ST-segment elevation myocardial infarction undergoing primary percutaneous coronary intervention. *LIPSIA-N.-ACC (Prospective, Single-Blind, Placebo-Controlled, Randomized Leipz. Immed. PercutaneouS Coron. Intervention Acute Myocard. Infarct. N.-ACC) Trial J. Am. Coll. Cardiol.* **55**, 2201–2209 (2010).
8. El-Hamamsy, I. et al. Effect of intravenous N-acetylcysteine on outcomes after coronary artery bypass surgery: a randomized, double-blind, placebo-controlled clinical trial. *J. Thorac. cardiovascular Surg.* **133**, 7–12 (2007).
9. Hausenloy, D. J. et al. Effect of remote ischaemic conditioning on clinical outcomes in patients with acute myocardial infarction (CONDI-2/ERIC-PPCI): a single-blind randomised controlled trial. *Lancet* **394**, 1415–1424 (2019).
10. Yu, J. et al. Histone lactylation drives oncogenesis by facilitating m(6)A reader protein YTHDF2 expression in ocular melanoma. *Genome Biol.* **22**, 85 (2021).
11. Wang, N. et al. Histone Lactylation Boosts Reparative Gene Activation Post-Myocardial Infarction. *Circ. Res* **131**, 893–908 (2022).
12. Xiong, J. et al. Lactylation-driven METTL3-mediated RNA m(6)A modification promotes immunosuppression of tumor-infiltrating myeloid cells. *Mol. Cell* **82**, 1660–1677.e1610 (2022).
13. Yang, Z. et al. Lactylome analysis suggests lactylation-dependent mechanisms of metabolic adaptation in hepatocellular carcinoma. *Nat. Metab.* **5**, 61–79 (2023).
14. Fan, M. et al. Lactate promotes endothelial-to-mesenchymal transition via Snail1 lactylation after myocardial infarction. *Sci. Adv.* **9**, eadc9465 (2023).
15. Zhang, D. et al. Metabolic regulation of gene expression by histone lactylation. *Nature* **574**, 575–580 (2019).
16. Pan, R. Y. et al. Positive feedback regulation of microglial glucose metabolism by histone H4 lysine 12 lactylation in Alzheimer's disease. *Cell Metab.* **34**, 634–648.e636 (2022).
17. Wang, X. et al. YY1 lactylation in microglia promotes angiogenesis through transcription activation-mediated upregulation of FGF2. *Genome Biol.* **24**, 87 (2023).
18. Sun, L. et al. Lactylation of METTL16 promotes cuproptosis via m(6)A-modification on FDX1 mRNA in gastric cancer. *Nat. Commun.* **14**, 6523 (2023).
19. Fan, W. et al. Global lactylome reveals lactylation-dependent mechanisms underlying T(H)17 differentiation in experimental autoimmune uveitis. *Sci. Adv.* **9**, eadh4655 (2023).
20. Zhang, N. et al. α-myosin heavy chain lactylation maintains sarcomeric structure and function and alleviates the development of heart failure. *Cell Res* **33**, 679–698 (2023).
21. Yu, W. et al. HSPA12A maintains aerobic glycolytic homeostasis and Histone3 lactylation in cardiomyocytes to attenuate myocardial ischemia/reperfusion injury. *JCI Insight* **9**, https://doi.org/10.1172/jci.insight.169125 (2024).
22. Angelidis, I. et al. An atlas of the aging lung mapped by single cell transcriptomics and deep tissue proteomics. *Nat. Commun.* **10**, 963 (2019).
23. Ichihara, G. et al. MRP1-Dependent Extracellular Release of Glutathione Induces Cardiomyocyte Ferroptosis After Ischemia-Reperfusion. *Circ. Res* **133**, 861–876 (2023).
24. Prag, H. A. et al. Ischemia-Selective Cardioprotection by Malonate for Ischemia/Reperfusion Injury. *Circ. Res* **131**, 528–541 (2022).
25. Gan, L. et al. Small Extracellular Microvesicles Mediated Pathological Communications Between Dysfunctional Adipocytes and Cardiomyocytes as a Novel Mechanism Exacerbating Ischemia/Reperfusion Injury in Diabetic Mice. *Circulation* **141**, 968–983 (2020).
26. Broadhurst, D. et al. Guidelines and considerations for the use of system suitability and quality control samples in mass spectrometry assays applied in untargeted clinical metabolomic studies. *Metabolomics: Off. J. Metabolomic Soc.* **14**, 72 (2018).
27. Lewis, M. R. et al. Development and Application of Ultra-Performance Liquid Chromatography-TOF MS for Precision Large Scale Urinary Metabolic Phenotyping. *Anal. Chem.* **88**, 9004–9013 (2016).
28. Want, E. J. et al. Global metabolic profiling procedures for urine using UPLC-MS. *Nat. Protoc.* **5**, 1005–1018 (2010).
29. Cheng, A., Grant, C. E., Noble, W. S. & Bailey, T. L. MoMo: discovery of statistically significant post-translational modification motifs. *Bioinforma. (Oxf., Engl.)* **35**, 2774–2782 (2019).
30. Macfelda, K. et al. Plasminogen activator inhibitor 1 expression is regulated by the inflammatory mediators interleukin-1alpha, tumor necrosis factor-alpha, transforming growth factor-beta and oncostatin M in human cardiac myocytes. *J. Mol. Cell Cardiol.* **34**, 1681–1691 (2002).
31. Chao, J., Guo, Y. & Chao, L. Protective Role of Endogenous Kallistatin in Vascular Injury and Senescence by Inhibiting Oxidative Stress and Inflammation. *Oxid. Med. Cell. Longev.* **2018**, 4138560 (2018).
32. Lauten, A. et al. Ischemia-reperfusion injury activates early extracellular matrix processing and expression of endostatin in the heart with differential effects of temperature. *Basic Res Cardiol.* **104**, 559–569 (2009).
33. Horvath, A. J. et al. The murine orthologue of human antichymotrypsin: a structural paradigm for clade A3 serpins. *J. Biol. Chem.* **280**, 43168–43178 (2005).
34. Delrue, L. et al. Circulating SERPINA3 improves prognostic stratification in patients with a de novo or worsened heart failure. *ESC Heart Fail.* **8**, 4780–4790 (2021).
35. Zhao, L. et al. Circulating Serpina3 levels predict the major adverse cardiac events in patients with myocardial infarction. *Int J. Cardiol.* **300**, 34–38 (2020).
36. Gettins, P. G. Serpin structure, mechanism, and function. *Chem. Rev.* **102**, 4751–4804 (2002).
37. Dai, X., Lv, X., Thompson, E. W. & Ostrikov, K. K. Histone lactylation: epigenetic mark of glycolytic switch. *Trends Genet.* **38**, 124–127 (2022).
38. Ding, R., Wu, W., Sun, Z. & Li, Z. AMP-activated protein kinase: An attractive therapeutic target for ischemia-reperfusion injury. *Eur. J. Pharmacol.* **888**, 173484 (2020).
39. Zhang, B. et al. Blocking the Wnt pathway, a unifying mechanism for an angiogenic inhibitor in the serine proteinase inhibitor family. *Proc. Natl Acad. Sci. USA* **107**, 6900–6905 (2010).

40. Hausenloy, D. J. & Yellon, D. M. New directions for protecting the heart against ischaemia-reperfusion injury: targeting the Reperfusion Injury Salvage Kinase (RISK)-pathway. *Cardiovasc. Res.* **61**, 448–460 (2004).

41. Lecour, S. Activation of the protective Survivor Activating Factor Enhancement (SAFE) pathway against reperfusion injury: Does it go beyond the RISK pathway? *J. Mol. Cell Cardiol.* **47**, 32–40 (2009).

42. Hausenloy, D. J. & Yellon, D. M. Reperfusion injury salvage kinase signalling: taking a RISK for cardioprotection. *Heart Fail Rev.* **12**, 217–234 (2007).

43. Lecour, S. et al. Pharmacological preconditioning with tumor necrosis factor-alpha activates signal transducer and activator of transcription-3 at reperfusion without involving classic prosurvival kinases (Akt and extracellular signal-regulated kinase). *Circulation* **112**, 3911–3918 (2005).

44. Suleman, N., Somers, S., Smith, R., Opie, L. H. & Lecour, S. C. Dual activation of STAT-3 and Akt is required during the trigger phase of ischaemic preconditioning. *Cardiovasc Res* **79**, 127–133 (2008).

45. Lecour, S. Multiple protective pathways against reperfusion injury: a SAFE path without Aktion? *J. Mol. Cell Cardiol.* **46**, 607–609 (2009).

46. Oshima, Y. et al. STAT3 mediates cardioprotection against ischemia/reperfusion injury through metallothionein induction in the heart. *Cardiovasc Res* **65**, 428–435 (2005).

47. Heusch, G., Musiolik, J., Gedik, N. & Skyschally, A. Mitochondrial STAT3 activation and cardioprotection by ischemic postconditioning in pigs with regional myocardial ischemia/reperfusion. *Circ. Res.* **109**, 1302–1308 (2011).

48. Wu, Q. et al. Cardiac protective effects of remote ischaemic preconditioning in children undergoing tetralogy of fallot repair surgery: a randomized controlled trial. *Eur. Heart J.* **39**, 1028–1037 (2018).

49. Owais, K. et al. Cardiopulmonary Bypass Decreases Activation of the Signal Transducer and Activator of Transcription 3 (STAT3) Pathway in Diabetic Human Myocardium. *Ann. Thorac. Surg.* **100**, 1636–1645 (2015).

50. Rabinowitz, J. D. & Enerbäck, S. Lactate: the ugly duckling of energy metabolism. *Nat. Metab.* **2**, 566–571 (2020).

51. Lazzeri, C., Valente, S., Chiostri, M., Picariello, C. & Gensini, G. F. Lactate in the acute phase of ST-elevation myocardial infarction treated with mechanical revascularization: a single-center experience. *Am. J. Emerg. Med.* **30**, 92–96 (2012).

52. Frydland, M. et al. Lactate is a Prognostic Factor in Patients Admitted With Suspected ST-Elevation Myocardial Infarction. *Shock (Augusta, Ga.)* **51**, 321–327 (2019).

53. Suzuki, A. et al. Astrocyte-neuron lactate transport is required for long-term memory formation. *Cell* **144**, 810–823 (2011).

54. Colegio, O. R. et al. Functional polarization of tumour-associated macrophages by tumour-derived lactic acid. *Nature* **513**, 559–563 (2014).

55. Yang, L. et al. Lactate Promotes Synthetic Phenotype in Vascular Smooth Muscle Cells. *Circ. Res* **121**, 1251–1262 (2017).

56. Widgerow, A. D. Ischemia-reperfusion injury: influencing the microcirculatory and cellular environment. *Ann. Plast. Surg.* **72**, 253–260 (2014).

57. Flores-Vergara, R. et al. Communication Between Cardiomyocytes and Fibroblasts During Cardiac Ischemia/Reperfusion and Remodeling: Roles of TGF-β, CTGF, the Renin Angiotensin Axis, and Noncoding RNA Molecules. *Front. Physiol.* **12**, 716721 (2021).

58. Patston, P. A. Studies on inhibition of neutrophil cathepsin G by alpha 1-antichymotrypsin. *Inflammation* **19**, 75–81 (1995).

59. Murohara, T., Guo, J. P. & Lefer, A. M. Cardioprotection by a novel recombinant serine protease inhibitor in myocardial ischemia and reperfusion injury. *J. Pharmacol. Exp. therapeutics* **274**, 1246–1253 (1995).

60. Ji, J. J. et al. Kallistatin/Serpina3c inhibits cardiac fibrosis after myocardial infarction by regulating glycolysis via Nr4a1 activation. *Biochimica et. biophysica acta Mol. basis Dis.* **1868**, 166441 (2022).

61. Caccioppo, A. et al. Ischemia Reperfusion Injury: Mechanisms of Damage/Protection and Novel Strategies for Cardiac Recovery/Regeneration. *Int. J. Mol. Sci.* **20**, https://doi.org/10.3390/ijms20205024 (2019).

62. Zhai, P., Eurell, T. E., Cooke, P. S., Lubahn, D. B. & Gross, D. R. Myocardial ischemia-reperfusion injury in estrogen receptor-alpha knockout and wild-type mice. *Am. J. Physiol. Heart Circ. Physiol.* **278**, H1640–1647 (2000).

63. Schwartz, D. & Gygi, S. P. An iterative statistical approach to the identification of protein phosphorylation motifs from large-scale Data sets. *Nat. Biotechnol.* **23**, 1391–1398 (2005).

64. Colaert, N. et al. The Online Protein Processing Resource (TOPPR): a database and analysis platform for protein processing events. *Nucleic Acids Res* **41**, D333–337 (2013).

65. Mann, M. & Kelleher, N. L. Precision proteomics: the case for high resolution and high mass accuracy. *Proc. Natl Acad. Sci. USA* **105**, 18132–18138 (2008).

66. Becker, R. A., Chambers, J. M. & Wilks, A. R. *The New S Language*. (Chapman and Hall/CRC).

67. Yu, G., Wang, L. G., Han, Y. & He, Q. Y. clusterProfiler: an R package for comparing biological themes among gene clusters. *Omics: J. Integr. Biol.* **16**, 284–287 (2012).

68. Huang, da,W., Sherman, B. T. & Lempicki, R. A. Bioinformatics enrichment tools: paths toward the comprehensive functional analysis of large gene lists. *Nucleic Acids Res* **37**, 1–13 (2009).

69. Huang, da,W., Sherman, B. T. & Lempicki, R. A. Systematic and integrative analysis of large gene lists using DAVID bioinformatics resources. *Nat. Protoc.* **4**, 44–57 (2009).

70. Cline, M. S. et al. Integration of biological networks and gene expression data using Cytoscape. *Nat. Protoc.* **2**, 2366–2382 (2007).

71. Zhou, B. et al. Functional isolation, culture and cryopreservation of adult human primary cardiomyocytes. *Signal Transduct. Target. Ther.* **7**, 254 (2022).

72. Yuan, X. et al. THO Complex-Dependent Posttranscriptional Control Contributes to Vascular Smooth Muscle Cell Fate Decision. *Circ. Res* **123**, 538–549 (2018).

Acknowledgements

Author contributions

Le W. conceived the project, designed the study, performed most of the experiments, analyzed the data, and wrote the manuscript. D.L. performed animal experiments. F.Y. performed bioinformatic analysis. S.F. performed Seahorse experiments. C.T. isolated neonatal mouse cardiomyocytes. R.R. isolated human primary cardiomyocytes. M.Z. isolated human primary fibroblasts. X.W., W.F., and Z.H. provided surgical samples. B.J. provided funding. S.H. and Li W. provided funding, resources, and conceptual input. B.Z. supervised the study, provided funding, and wrote, edited and revised the manuscript.

Competing interests

The authors declare no competing interests.

Additional information